FEDERAL UNIVERSITY OF UBERLÃNDIA
MECHANICAL ENGINEERING FACULTY
AERONAUTIC ENGINEERING

# PROPELLER OPTIMIZATION APPROACH:
## Blade Element Momentum Theory in Accelerated Differential Evolution

*Author:*
Iago Tetsuo Nonaka

**Uberlândia**
**2023**

IAGO TETSUO NONAKA

# PROPELLER OPTIMIZATION APPROACH:
## Blade Element Momentum Theory in Accelerated Differential Evolution

Undergraduate Thesis presented to Faculty of Mechanical Engineering from the University Federal of Uberlândia in fulfillment of the requirements for the Bachelor's degree of Aeronautical Engineering.

*Evaluation board:*
João Marcelo Vedovotto - Advisor
Aldemir Aparecido Cavallini Junior
Alex José Elias

**Uberlândia**
**2023**

# ACKNOWLEDGEMENTS

I reserve my thanks to those who directly and indirectly contributed to my academic, professional, and, most importantly, personal growth. I wish you all success and achievements, with the certainty that they will come at the right time.

First of all, to my parents, for all their support, and for encouraging me to chase my dreams and believe in my potential. To my brother and sister, for accompanying me throughout this stage. For all my family who cared and worried about me.

To my friends, I thank you for all the moments of ups and downs experienced during graduation. Rest assured that I will cherish all the memories.

To the professors, for making the Public University a space for great debate, acceptance, and exchange of knowledge. Thank you for making the effort to transmit a portion of everything you know to us students, in addition to contributing to our education.

I would also like to thank Embraer S.A. for the opportunity to enter the aeronautical industry as my first professional experience and for all the learning I acquired.

Finally, I thank God for opening so many doors in my life and for allowing all the achievements.

# ABSTRACT

Newton's Third Law states that for every action, there is a reaction. The aircraft can propel itself by pushing air backward, it may propel a high quantity of air at a low speed, or a small quantity at higher velocities. Aircraft that operate at low Mach produce thrust by a combination of engine and propeller. Accurate propeller predictions are crucial in aircraft performance since further analysis would consist of computational simulations or experiments, which are highly time-consuming. In this thesis, an analytical method to improve the design and performance of a propeller is presented, using MATLAB. First, the implementation of Blade Element Momentum Theory, based on a database built by XFOIL. After validating the results with analytical and experimental results from other theses, an algorithm of optimization Accelerated Differential Evolution was implemented. The main objective is to create an approach, that defines an optimal airscrew that will best suit an engine. The results provided a propeller's higher efficiency of 4% compared to the one made for an electrical aircraft.



**Keywords:** propeller, blade, thrust, optimization.

# List of Figures

# List of Tables

# Symbols

| | |
|---|---|
| $\alpha$ | Angle of attack |
| $\alpha_s$ | Stall angle of attack |
| $a_x$ | Axial interference factor |
| $a_y$ | Rotational interference factor |
| $A$ | Area |
| $a$ | Acceleration |
| $\beta$ | Twist angle |
| $b_i$ | Bernstein i coefficient |
| $b$ | Bézier curve value |
| $B$ | Number of blades |
| $BEMT$ | Blade Element Momentum Theory |
| $\rho$ | Density of the fluid |
| $APR$ | Effective pitch |
| $c$ | Chord |
| $C_D$ | Total drag coefficient |
| $C_d$ | Drag coefficient |
| $C_{D_s}$ | Drag coefficient at stall angle |
| $C_L$ | Total lift coefficient |
| $C_l$ | Lift coefficient |
| $C_{L_s}$ | Lift coefficient at stall angle |
| $C_Q$ | Torque coefficient |
| $C_T$ | Thrust coefficient |
| $C_X$ | X force coefficient |
| $C_Y$ | Y force coefficient |
| $D$ | Drag force |
| $d$ | Diameter |
| $dT$ | Thrust per unit span |
| $dQ$ | Torque per unit span |
| $F$ | Force |
| $f$ | Prandtl-Glauert correction coefficient |
| $F_P$ | Prandtl tip loss factor |
| $H$ | Geometrical pitch |
| $J$ | Advance/diameter ratio |
| $K$ | Goldstein momentum loss factor |
| $L$ | Lift |
| $lb$ | Lower boundary admitted for optimization variables |
| $M$ | Momentum force |
| $N$ | Normal force |
| $n$ | Number of stations |
| $n_s$ | Rotations per second |
| $N_B$ | Number of Bézier control points |
| $M$ | Mach number |
| $P_A$ | Available power |
| $P_R$ | Required power |
| $P_i$ | Bézier control point i |
| $t$ | Bézier parameter |

| | |
|---|---|
| $T$ | Total thrust |
| $THP$ | Thrust Horsepower |
| $BHP$ | Brake Horsepower |
| $HP$ | Horsepower |
| $Q$ | Total torque |
| $R$ | Resultant Force |
| $R_{cut_off}$ | Cut-off radius |
| $Re$ | Reynolds number |
| $\Omega$ | Engine rotational speed |
| $RAF$ | Relative air flow |
| $SFC$ | Specific Fuel Consumption |
| $T$ | Thrust |
| $ub$ | Upper boundary admitted for optimization variables |
| $V$ | Speed |
| $V_\infty$ | Relative speed |
| $V_X$ | Axial flow speed |
| $V_Y$ | Radial flow speed |
| $W$ | Module of airflow speed |
| $\gamma$ | Parameter of Fobj |
| $\epsilon$ | Difference of W between interations |
| $\eta$ | Efficiency |
| $\eta_{cruise}$ | Efficiency in cruise conditions |
| $\eta max$ | Maximum efficiency |
| $\theta$ | Blade pitch |
| $\xi$ | Non dimensional radius |
| $\sigma$ | Blade solidity |
| $\phi$ | Inflow angle |
| $\nu$ | Kinematic viscosity |
| $\phi_{new}$ | Inflow angle in new iteration |
| $\phi_t$ | Inflow angle at the tip |
| $\omega$ | Angular velocity |

# Contents

# 1 Introduction

The purpose of this thesis is to develop an approach to predict an optimal propeller (or fan) for engines that operate in low Mach with its main parameters: torque and RPM. Blade Element Momentum Theory (BEMT) and Accelerated Differential Evolution (ADE) are combined to achieve this goal, resulting in low-consuming processing. A validation of BEMT was achieved after comparing the results to analytical and experimental results from other theses. On the one hand, there exists software on the web that provides analytical results for the thrust and torque required. On the other, they do not specifically define an optimal design for a specific engine, or the propeller's parameters to achieve the result.

The main advantage of developing this program is the possibility of defining the blade geometries constraints to a specific case, and still getting an optimum result. For example, some aircraft have a propeller's diameter limitation because of their structure, or the goal is not efficiency, but the thrust. Machine Learning provides the capability to define the best set of parameters in the earlier stages of aircraft development, which will reduce the time consumed to design an optimum propeller given the conditions imposed. It makes the code much more versatile than other programs.

Firstly, is mandatory to obtain the capability of understanding the fundamentals before calculating propeller performance. To do this, the basic content of fluid mechanics, aerodynamics, and propulsion are considered. Then, the propeller aspects and classification are explained.

Following, the BEMT equations are presented and briefly the Machine Learning concept is shown to explain the reason that ADE was chosen. To validate the BEMT algorithm, a comparison between analytical and experimental results is made. Once the model is set up, the implementation of ADE is possible.

Finally, the ADE results are discussed in Chapter 7, and conclusions on the work performed along with recommendations for future studies are described in Chapter 8.

# 2 Fundamentals

To understand the propeller's performance, it's necessary to understand all the characteristics of an aircraft, so a basic understanding of aeronautical engineering is presented.

## 2.1 Fluid Mechanics

Çengel [16] defines fluid as a substance in the liquid or gas phase as a fluid. The distinction between a solid and a fluid is made based on the substance's ability to resist an applied shear (or tangential) stress that tends to change its shape.

Therefore, it's necessary to classify the work fluid for this document:

- Internal or external: depending on the fluid flows in a confined space or over a surface;
- Compressible or incompressible: depending on the level of variation of density during flow, incompressibility is an approximation made to simplify the calculus, in which the flow is said to be incompressible if the density remains nearly constant throughout the motion ;
- Laminar, transitional or turbulent: depending on the disorder of the fluid, the Reynolds Number ($Re$) is a parameter established to determine the flow regime at each point, as shown in Figure 1;
- Unsteady or steady: the steady and uniform flow implies no change of properties, like velocity, temperature, etc., and the unsteady, is the opposite, also called transient, that is typically used for developing flows.

Figure 1: Laminar, transitional, and turbulent flows over a flat plate.

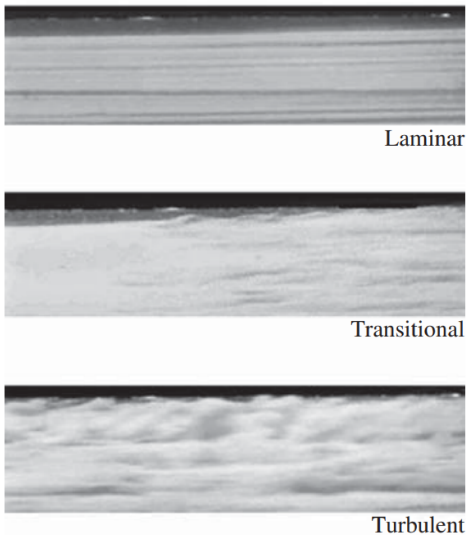


Source: Çengel [16]

For this research, the assumptions of an external, incompressible, laminar, and steady flow were made. The flow near the blades of the propeller is unsteady, but for airscrew, it's considered the overall flow field rather than the details.

## 2.2 Aerodynamics

The study of the dynamics of both liquids and gases under the same general heading is called fluid dynamics. Certain differences exist between the flow of liquids and the flow of gases; also, different species of gases have different properties. Therefore, fluid dynamics is subdivided into three areas as follows:

- Hydrodynamics: flow of liquids
- Gas dynamics: flow of gases
- Aerodynamics: flow of air

As there are many similarities and identical phenomena between them, the word "aerodynamics" has taken on a popular usage that sometimes covers the other two areas. Aerodynamics is an applied science that studies the properties of moving air and the interaction between this fluid and solid bodies moving through it.

Figure 2: Ilustration of Flow Velocity and Streamlines

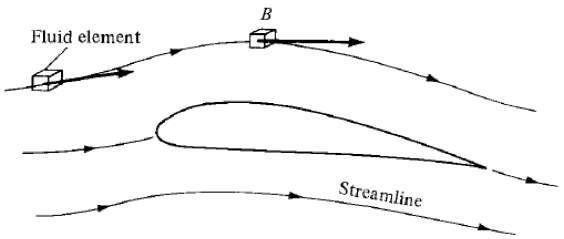


Source: Anderson [3]

The section of a wing represented in Figure 2 is designed to produce the best relation between lift and drag for each situation. In this Image, the Lift force is upward and is the primary force for lifting the aircraft in the air, thus, it must be maximized. Drag force always acts as a counter-motion force, thus, it must be minimized.

In airplanes, there are four major forces: lift, drag, thrust, and weight. Which are represented by Figure 3.

Figure 3: The major forces in airplanes.

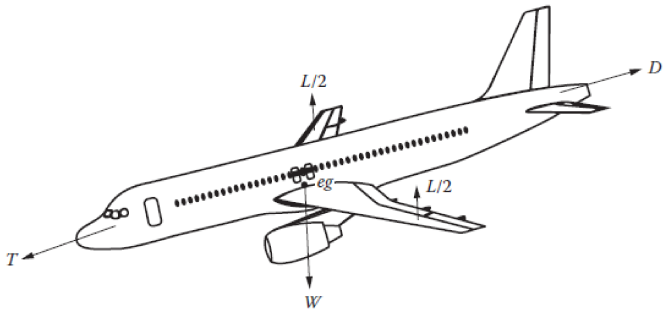


Source: Anderson [3]

Focusing on the wing's section, the aerodynamic forces could be illustrated in Figure 4, the moment caused by this movement can make the construction of the wing difficult, since the objective of the wing is to generate less drag. Then, it has to be evaluated during the aircraft's conceptual process to provide the structural resistance necessary.

Figure 4: Resultant aerodynamic force and moment on the airfoil.

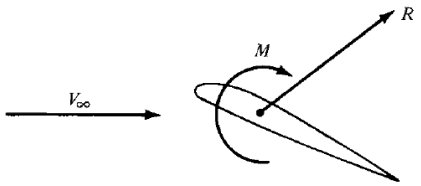


Source: Anderson [3]

Regardless, the main forces can be represented by Figure 5, the Lift is the perpendicular force relative to the relative velocity($V_\infty$), while the Drag's component is parallel.

Figure 5: Component of aerodynamic forces.

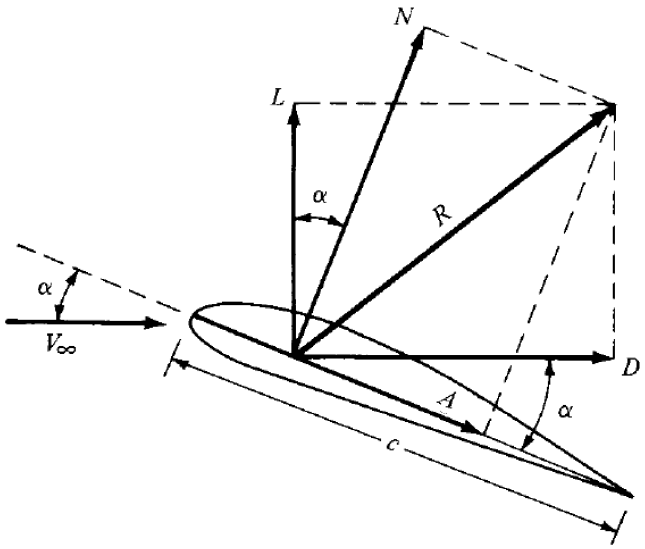


Source: Anderson [3]

- The chord ($c$) is the linear distance from the leading edge to the trailing edge of the body;
- The angle of attack ($\alpha$) defined as the angle between $c$ and $V_\infty$.

Sometimes the component $R$ is divided into two major forces: $N$ normal force, the component perpendicular to $c$, and $A$ axial force, the component parallel to $c$. The last dimension that has to be mentioned is the span ($l$).

Figure 6: Main airfoil geometrical parameters.

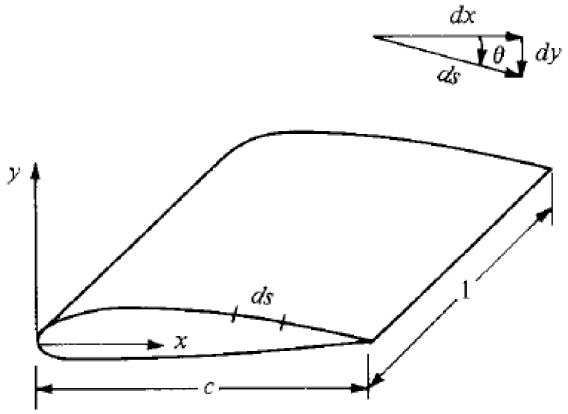


Source: Anderson [3]

### 2.2.1 Drag

As explained earlier, there are two forces most utilized to understand airfoil performance, Drag and Lift, the first one is calculated by the following formula:

$$D = \frac{\rho V^2 C_D A}{2} \tag{1}$$

where

- Drag force($D$);
- Density of the fluid($\rho$);
- The speed of the object relative to the fluid($V$);
- The cross-sectional area($A$);
- Drag coefficient($C_D$);

The drag is classified into 2 types: Parasite and Induced Drag. The parasite is made out of Interference Drag, Friction Drag, and Form Drag.

- Form Drag: A body that moves through the fluid displaces it. Each aspect as roughness and thickness will more or less increase or decrease Drag as the streamlined body with low thickness will have small drag.;

- Skin Friction Drag: since air immediately attached to a body has null flow speed due to friction forces and viscosity. Surface friction causes heating of the outer skin of a body, leading to a loss of kinetic energy in thermal;
- Interference Drag: different components on a body impose aerodynamic interference, for example where the wings are attached to the fuselage (wing structures, etc).

Induced drag is the result of pressure equalization between the high pressure under the wing and the low pressure above the wing. In other words, parasite drag is all the drag independent of the lift, while the induced drag is formed due to the lift.

Figure 7: Parasite Drag and Induced Drag effect with Speed.

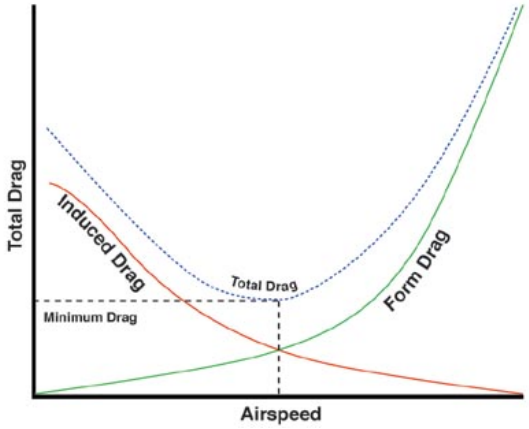


Source: ANAC [1].

## 2.3 Propulsion

The powertrain is designed to produce thrust, mainly by Newton's Third Law: Action and Reaction. The idea is to generate a force forward pushing back the airflow that passes from the engine at a higher velocity. In an airbreathing engine, a mixture of air and fuel generates power through combustion. This energy will produce thrust directly or it will be converted to axis power to activate a mechanism that pushes a higher quantity of fluid.

The propeller or fan cooperates with the engine producing this increase of intake airflow to reduce the necessity to speed up the exhaustion gas. However, this concept of interaction won't be discussed in this document. In short, the propeller is used on piston, turboprop, and turboshaft engines [12].

According to Sadraey [12], each engine type has the best condition to operate, and the ones that contain propellers have an optimal performance at low-velocity operation at lower altitudes. These engines have a maximum velocity, due to their limitation of $RPM$. At one point the propeller cannot produce higher thrust due to the relative airspeed, so the airplane won't accelerate and will reach maximum operating speed, as Figure 8 shows that the turboprop's efficiency drops significantly.

Figure 8: Engines typical propulsion efficiency.

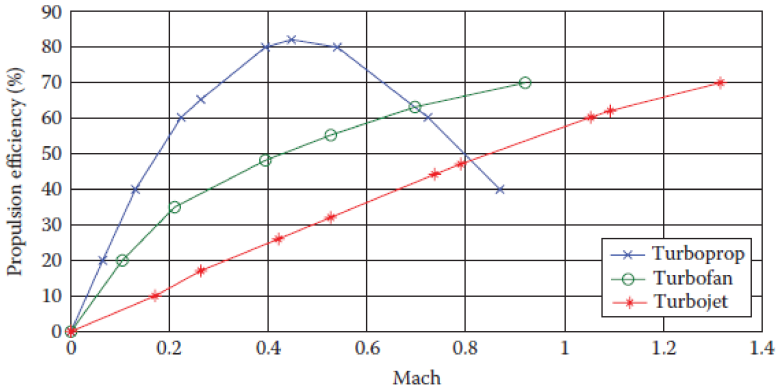


Source: Sadraey [12].

Figure 9: A comparison between operating limits of various engines.

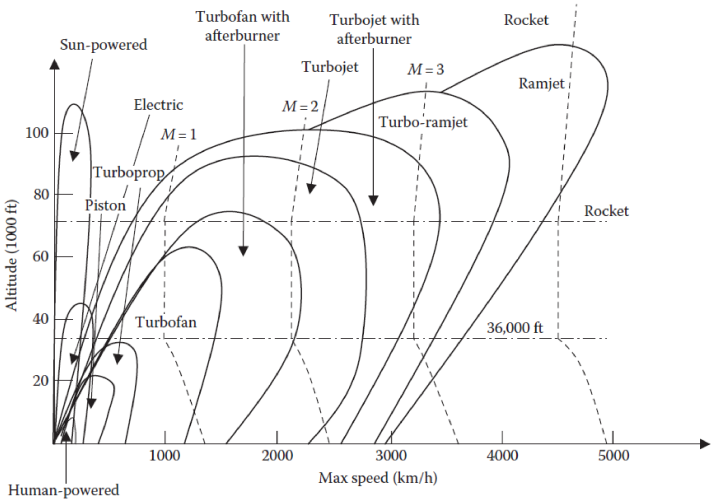


Source: Sadraey [12].

Prop-driven engines are mostly used on small and medium-sized aircraft, generally more efficient at speeds below $201[m/s]$. On short take-off and landing (STOL) aircraft and short-haul regional routes, the difference in flight time compared to a long flight becomes evident. These prop-driven engines consume approximately $1/3$ less fuel in regional flights, compared to jets, so they are more profitable in short flights.

Thus, propulsion directly affects the aircraft's performance. There are two types of longitudinal power generated by the aircraft, the Power Available ($P_A$) and the Power Required ($P_R$). The first one is the output power of the engine-propeller combination, while the second is the power required to maintain an unaccelerated flight. So, Required Power is directly related to Drag, Sadraey [12] defines it as "the engine power required for a specific mission". Considering thrust force ($T$) by aircraft speed ($V$), it can be calculated by the following formula:

$$P_A = TV \tag{2}$$

$$P_R = T_{Req}V = DV \tag{3}$$

Figure 10: Typical variations of specific fuel consumptions($SFC$) along Mach number.

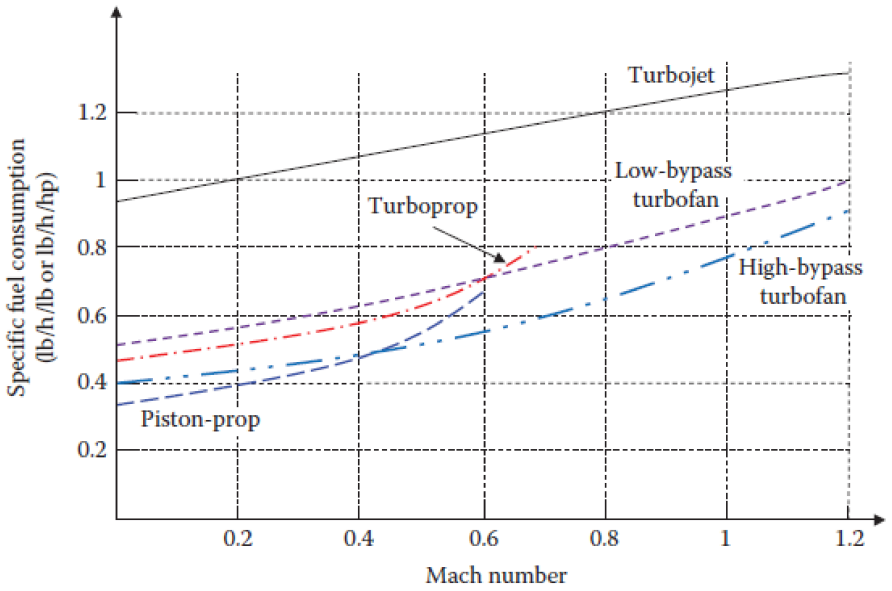


Source: Sadraey [12].

Figure 11 represents the velocities studied by Aircraft Performance Engineers to provide instruction to the pilots and define the best conditions of flight for each stage. However, there's no need to explain these velocities, this Subchapter was meant to explain the impact of a propeller.

Figure 11: Available power vs Required power of an aerodesign model.

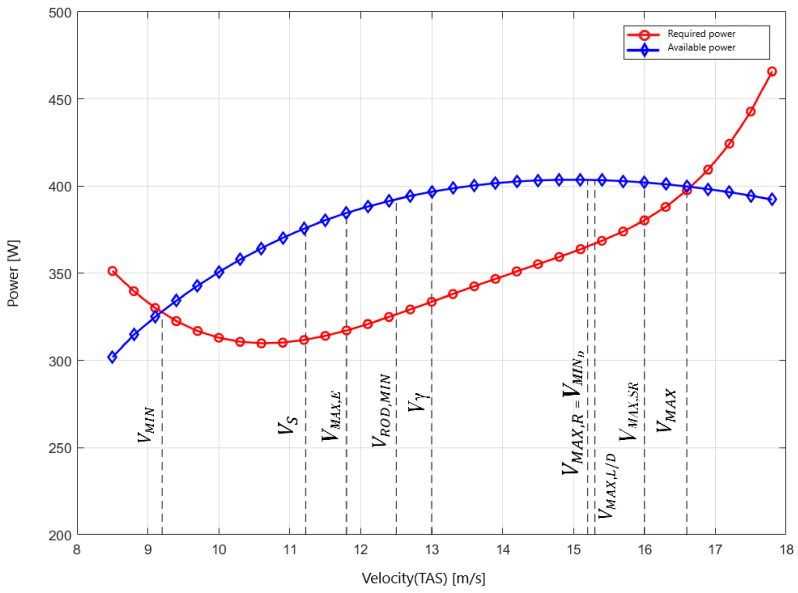


Source: Own authorship.

# 3 Propeller

A propeller is a device that causes a ship or aircraft to move, consisting of two or more blades that spin at high speed. Its purpose is to convert the engine torque into axial thrust, or propwash.

As explained in Subsection 2.3, the propeller pushes the working fluid which is the volume of air. The blade is an airfoil and works similarly to the wing, but as it rotates, the working fluid is at a higher velocity along the root to tip. It accompanies the need for a twist to have an optimum attack angle, including many other variables that will be presented. Therefore it's indispensable to understand propeller parameters and classification.

Figure 12: Propeller angles and aerodynamic forces.

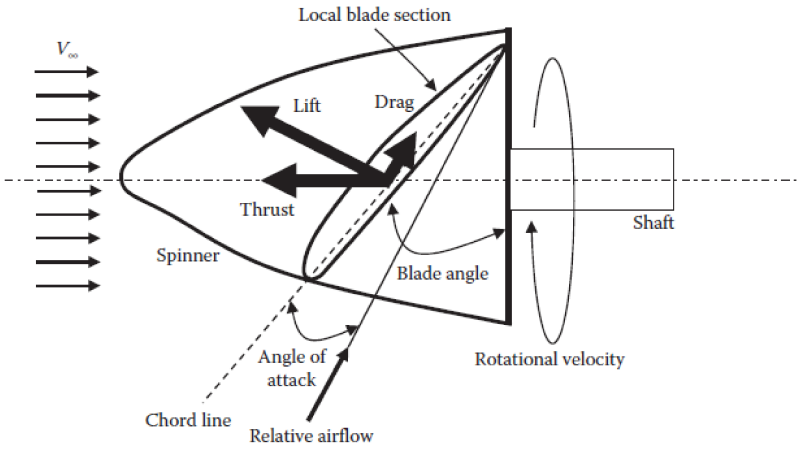


Source: Sadraey [12]

## 3.1 Propeller Properties

### 3.1.1 Propeller Terminology

- Blade element: theoretically thin cross-section of the prop blade and is perpendicular to the blade's major axis. The blade profile is the shape of this cross-section of the blade;
- Propeller's back: the curved, upper surface; to better understand, this part of the prop is viewed from in front of the aircraft;
- Prop blade: relatively flat surface corresponds to the wing's under surface, thrust face, or pressure face due to this side of the propeller producing air pressure above ambient;
- Shank: located at the blade root and being circular, it is designated to give strength to the blade. It plays no part in producing thrust, although it does produce drag. It's important to notice that not all propellers have shanks;
- Propeller's boss: the thick central non-aerodynamic part of a wooden fixed-pitch prop, it transmits the power delivered from the engine;

- Hub: the same central position as the boss but is a separate unit to which the blades and constant-speed unit are attached;
- Spinner: the streamlined fairing covering the hub area. On some aircraft, it is used for aesthetic reasons or it may also be an essential item on other aircraft to smooth the airflow into the engine air intakes, and reduce drag;
- Prop blade's leading and trailing edges plus the tips and roots, all share the same terminology as applied to an aircraft wing;
- Blade cuff: located at the blade root to enhance airflow into the engine intakes and for greater propeller solidity.

Figure 13: Propeller angles.

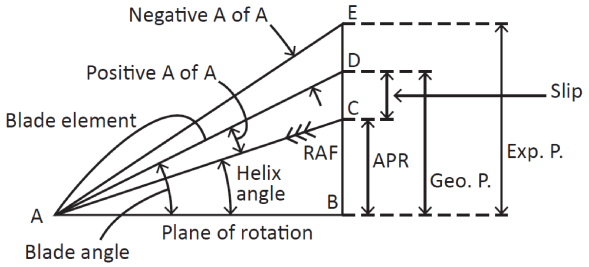


Source: Hitchens [7]

Figure 13 shows the relationship of the blade's notable points:

- helix angle: AB–AC;
- the blade angle: AB–AD;
- the angle of attack: AC–AD;
- the advance per rev: B–C;
- the geometric pitch: B–D;
- the slip: C–D;
- the experimental pitch: B–E;
- the prop's axial (or forward) component: B-E;
- the tangential component or plane of prop rotation: A-B;
- Relative air flow (RAF).

### 3.1.2 Propeller Pitch

The angle between the relative velocity and the plane of the propeller rotation is called the helix angle of advance. For a particular airplane velocity, the helix angle varies from the root to the tip since the propeller tip revolves faster than the root sections; the helix angle approaches 90° at the blade root. The blade angle or the pitch angle is the total angle from the plane of the propeller rotation to the chord line of the blade section, which is the sum of the helix angle and angle of attack for that section.

When a screw rotates, it will advance a given distance in each turn equal to its pitch; in other words, its advance per revolution is a fixed quantity equal to its pitch. The geometric pitch of the screw is the distance between each adjacent thread.

Under certain operating conditions of aircraft forward speed and prop RPM, the advance per rev equals the geometric pitch.

Figure 14: Propeller geometric pitch.

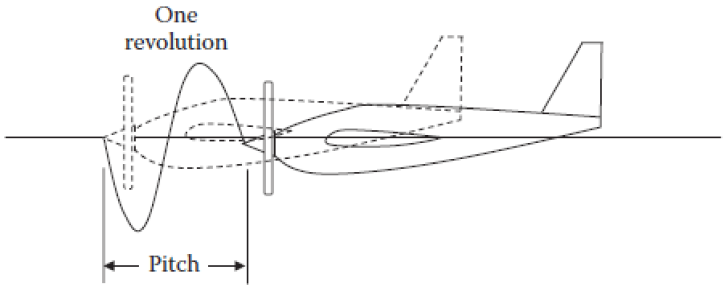


Source: Sadraey [12]

For this thesis, it will be assumed that the given blade section works on a fixed-pitch propeller (the simplest propeller which will be presented further) where the geometric pitch and experimental pitch both remain constant and the advance per rev and slip are variables.

### 3.1.3 Helix Angle

The helix angle which is also known as the angle of advance, is the angle between the propeller's plane of rotation and the resultant direction of the relative airflow, vector AC in Figure 13.

When the engine is operational, the propeller rotates with a velocity vector (A-B) as shown in Figure 13. During this rotation, the propeller covers a circumferential distance equal to $2\pi R$, where R represents the radius. This rotational velocity is commonly referred to as the tangential velocity.

Simultaneously, when the aircraft is in motion, it acquires a forward velocity along the axial vector component. This forward movement results in the propeller covering a specific distance per revolution, known as the 'advance per rev' or 'effective pitch,' within a given unit of time. The magnitude of this advance per rev depends on the forward speed of the aircraft.

Any alteration in the propeller's RPM or the advance per rev brings about a change in the helix angle. The blade element chosen follows a helical flight path represented by vector A-C. The helix angle is directly related to the advance per rev or effective pitch.

In summary, when the engine is running, the propeller's rotational velocity, forward velocity of the aircraft, and helix angle all interact to determine the propeller's performance characteristics.

The helix angle is calculated by the following formula:

$$tan(\theta) = \frac{APR}{2\pi r} \tag{4}$$

- Axial component or effective pitch (APR);
- Prop radius (r);

Therefore, the effective pitch can be found from the formula:

$$APR = 2\pi r.tan(\theta) \tag{5}$$

### 3.1.4 Blade Angle and Twist

The blade angle is defined as the angle between the propeller's plane of rotation (A–B) in Figure 13, Propeller Terminology, and the prop blade's chord line (A–D) combing the helix angle plus the angle of attack. It has the same meaning as a wing's angle of attack [7].

To produce the maximum lift/drag ratio, each blade section must have a small angle attack of 3 to 4 degrees. To achieve this constant angle of attack, along the length of the blade, the propeller blade must be twisted. This is known as the propeller's geometric twist where the angle between the blade chord and its plane of rotation varies along the blade's length. This requires the blade angle to be greater at the root with a gradual reduction towards the tip, as mentioned above. The geometric pitch of the propeller then remains constant due to the blade angle decreasing with an increase in blade radius. The actual blade twist is designed to provide the correct angle of attack at the design cruise speed, which normally is the most durable flight phase.

### 3.1.5 Experimental Pitch

The experimental pitch refers to the propeller's advance per revolution when it generates zero net thrust. Figure 15, Experimental Pitch, illustrates that as the advance per rev (APR) increases from point B to E, the angle of attack decreases until it reaches a negative angle (AD-AE), causing the blade section to stop producing thrust. In this state, the relative airflow aligns along the line from E to A, similar to the wing's 'zero lift line,' and becomes the propeller's zero thrust line.

From a designer's perspective, the experimental pitch is regarded as the 'ideal pitch' because it possesses a distinct value and length determined by the propeller's characteristics. This pitch can be utilized for experimental measurements, hence its name [7].

In summary, the experimental pitch represents the advance per revolution at which the propeller ceases to generate net thrust. It serves as an important reference point for designers and can be employed for experimental purposes due to its well-defined value and length.

Figure 15: Experimental pitch diagram.

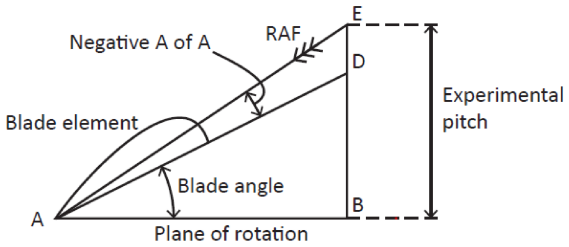


Source: Hitchens [7]

A fixed-pitch propeller has only one experimental pitch, while a constant-speed prop's pitch is variable over the available operating range of the blade angles between the fine and coarse pitch stops. The experimental pitch may also be known as the 'zero thrust pitch' or the 'exponential mean pitch'.

### 3.1.6 Geometric Pitch

The geometric pitch refers to the distance covered by the propeller in a single revolution when the blades' angle of attack is set to zero degrees.

Figure 16: Geometric Pitch diagram.

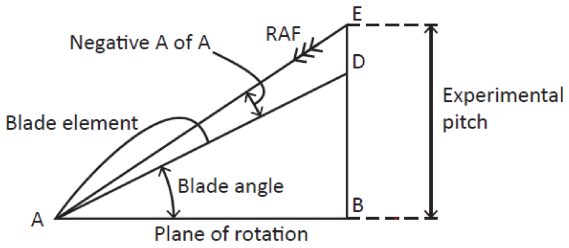


Source: Hitchens [7]

The geometric pitch ($H$) is found when the prop is advancing with zero degrees angle of attack, it's equal to the advance per rev. To maintain a constant pitch, the angle of each blade section must increase from the blade tip to the blade root to obey the law. The equation below should hold true for the whole length of the prop blade. However, if it doesn't unfold, the geometric pitch is stated for one section of the blade only at the 'standard radius; this point is located at the 70% station along the blade span. It's possible to find the geometric pitch of a propeller in inches as follows:

$$tan\beta = \frac{H}{2\pi r} \tag{6}$$

Upon examining Figure 16, which illustrates the Geometric Pitch, one can observe a slight presence of slip. Even at a zero-degree angle of attack, the propeller's curved back generates a small amount of thrust. Typically, the geometric pitch is lower than the experimental pitch, although exceptions to this rule may exist.

Figure 17: Propeller Pitches Lift Coefficient vs Angle of Attack.

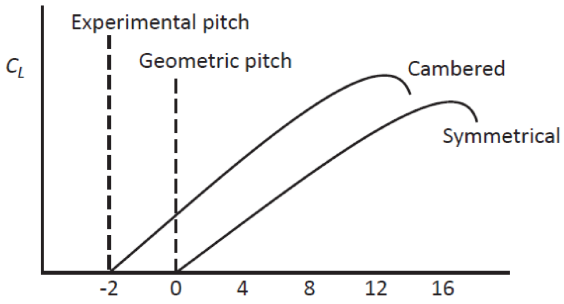


Source: Hitchens [7]

In a similar analogy, the propeller blades can be likened to the wings and tailplane of an aircraft. While the vertical tail features a symmetrical airfoil with equal curvature on both sides, most aircraft (except for aerobatic ones) have a cambered main wing. The cambered airfoil exhibits a greater curvature on the upper surface compared to the lower surface, similar to the shape of propeller blades.

Figure 17, showcasing the Lift Coefficient V. Angle of Attack, reveals that a symmetrical airfoil section ceases to generate lift at a zero-degree angle of attack. However, what is of particular interest here is that, at a zero-degree angle of attack, the cambered airfoil continues to generate lift (or thrust in the case of the propeller), as indicated by a positive lift coefficient. This corresponds to the propeller's geometric pitch.

Further reducing the angle of attack to minus two or three degrees eventually results in a zero lift coefficient, known as the angle of zero lift for the wing or the angle of zero thrust for the propeller. This corresponds to the propeller's experimental pitch.

### 3.1.7 Slip

The 'slip' of the propeller can be defined as the 'difference between the advance per rev and the geometric pitch'. When the advance per revolution matches the experimental pitch, a slightly negative angle of attack is present, resulting in zero thrust. However, under normal operating conditions, the angle of attack typically ranges around positive three degrees, while the advance per revolution is significantly less than the geometric pitch.

In Figure 16, Geometric Pitch, it can be observed that the combination of the advance per revolution (B-C) and the slip (C-D) equals the geometric pitch (B-D). In order for the propeller to achieve maximum thrust and efficiency, slip is necessary due to the fact that air is not a solid medium. Maximum efficiency is attained when the slip, expressed as a percentage, is approximately 30% of the length of the geometric pitch. In other words, slip represents the difference between the actual distance the propeller travels forward in one revolution (B-C or effective pitch) and the distance it would theoretically cover in one

revolution if its advance per revolution were equal to the geometric pitch (B-D). Slip is expressed as a percentage of distance.

Given the prop RPM, prop pitch in inches, and true airspeed in knots, the slip can be found using the following formula:

$$Slip = \frac{RPM.H.60}{6080.12} \tag{7}$$

It must be emphasized that slip is related to the geometric pitch and the advance per rev. Figure 16, shows a small amount of slip (C–D) is present when the prop blades are operating at zero angle of attack (geometric pitch). To produce thrust, the slip must be present with the maximum prop efficiency occurring at around 30% slip or 30% of the geometric pitch.

### 3.1.8 Advance/Diameter Ratio

The aircraft designer faces the task of selecting the propeller that possesses the most appropriate pitch and diameter for the specific aircraft, its intended mission, and the design airspeed. When presented with a range of propellers, each with blade angles increasing in a systematic order, a helpful parameter to consider is the advance/diameter ratio. This ratio allows for the characterization of a propeller using a non-dimensional form.

The advance/diameter ratio, denoted as J, is defined as the quotient of the aircraft's True Air Speed (TAS) and the product of the propeller's RPM and diameter. By employing this ratio, designers can effectively assess and compare the performance attributes of different propellers, taking into account the specific requirements and characteristics of the aircraft.

$$J = \frac{V}{\Omega d} \tag{8}$$

- Advance/diameter ratio(J);
- RPM($\Omega$);
- Propeller diameter(d).

In Figure 18, the Advance/diameter Ratio plot illustrates the relationship between the advance/diameter ratio and efficiency for a range of propellers with increasing pitch. The numbers displayed above the curves indicate the blade angles for each propeller. Efficiency exhibits an upward trend as the ratio increases, but only up to a certain threshold. When the ratio becomes too high, the angle of attack of the blades surpasses the stalling angle at lower forward speeds, resulting in a decrease in available thrust for take-off. Decreasing the propeller's diameter also decreases efficiency by placing excessive strain on the propeller blades.

A fixed-pitch propeller's efficiency curve shifts to the left when RPM and True Air Speed (TAS) decrease, and to the right when RPM and TAS increase. Furthermore, Figure 18 showcases the efficiency curves for a fine/flat pitch propeller (10 degrees) and

a coarse pitch propeller (40 degrees). The majority of single-engine light aircraft employ propellers that fall between these two extremes. In contrast, a constant-speed propeller offers an infinite number of curves within the range of fine and coarse pitch limits, allowing the pilot to select the optimal setting for climb or cruise.

Slip function and effective pitch are alternate names for the advance/diameter ratio.

Figure 18: Advance/diameter ratio.

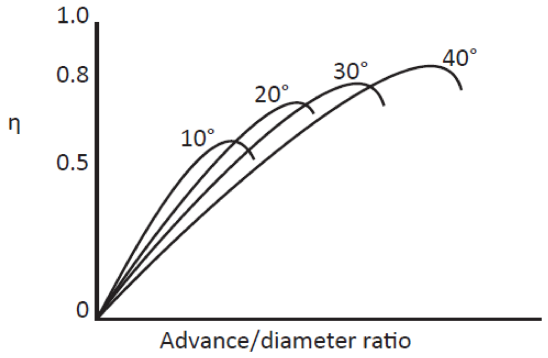


Source: Hitchens [7]

## 3.2 Propeller Classifications

Sadraey [12] separates the 3 types of propellers. Fixed-pitch propeller, the simplest type of propeller that exists is the cheapest to install and maintain. Due to the absence of a constant-speed unit (CSU) which is the design feature to better utilize the power produced by the engine, the disadvantage is the maximum efficiency at only one airspeed, so it's better for aircraft that operate at low speed.

The second, variable pitch propeller, as engines with greater horsepower were developed to operate at greater cruise speeds, the fixed-pitch props suffered in performance. So, a variable-pitch (VP) in 1916 occurred the first try-out in an airship, an airscrew with forward and reverse thrust to help with maneuvering. After, it was able to change the pitch long axis (coarse to fine or any angle between) to change the blade pitch during the flight controlled by the pilot, which was called a controllable-pitch propeller.

Controlling the blade pitch, allows the pilot to set the attack angle. To provide the best lift-drag ratio.

Figure 19: Fine pitch.

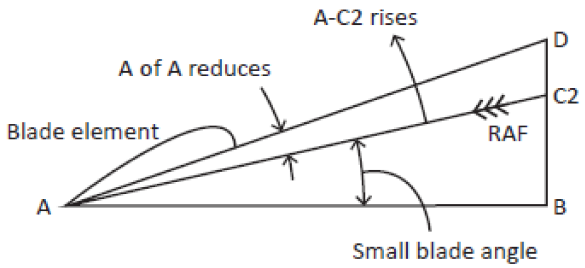


Source: Hitchens [7]

Figure 20: Coarse pitch.

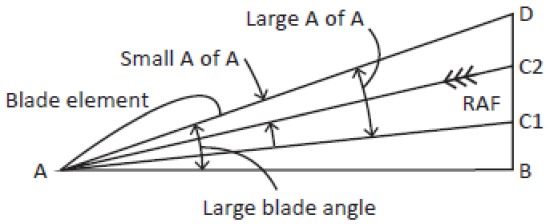


Source: Hitchens [7]

The last one, the constant-speed propeller was patented in 1924, the main idea is to not depend on the pilot during the flight to control the blade pitch, he only sets the desired engine speed. So, the aircraft's best performance is assured by the CSU, which controls the propeller's governor to change the blade pitch automatically.

The main benefit of the constant speed propeller is that it provides peak performance in every phase of flight from take-off to landing, the pilot can select the RPM that provides the most suitable power for any situation, it improves fuel efficiency and reduces train from the engine.

## 3.3 Thrust and Efficiency

As already explained propeller's purpose is to convert the engine torque into axial thrust, the objective of this chapter is to detail how it's possible to obtain the maximum thrust/brake power ratio. Propeller efficiency can be defined as:

$$\eta = \frac{THP}{BHP} \tag{9}$$

Thrust Horsepower (THP) is the power that is imparted by the propeller to the air, while brake horsepower (BHP) is the horsepower actually delivered to the output shaft. The horsepower (HP) is calculated by the product of $torquexRPM$, just to clarify, the equation to calculate horsepower is:

$$HP = \frac{\Omega Q}{5,252} \tag{10}$$

The propeller efficiency is defined as, the coefficient between useful power, and propeller power required. Now, it's possible to measure this by decomposing the Equation 9 with the already stated in Subchapter2.3, considering torque needed ($Q$) at a rotational speed of the engine ($\Omega$). It's important to note that this power required is different from the power required there 2.3.

$$\eta = \frac{P_A}{P_R} = \frac{TV}{\Omega Q} \tag{11}$$

The choice of this definition is not arbitrary. In the case of helicopters, where a hover flight condition is possible, this definition should be changed and written after a different figure of merit, since in hover, the airspeed far from the disk is zero, and, therefore,

the efficiency would be null too. Other equations to analyze propeller performance are explained further.

First of all, the propeller's material can change substantially the efficiency, as the propeller tends to be thinner to present better aerodynamics, there are two parameters that influence this choice: the structural strength and the weight. So, the composite is the best option currently.

Figure 21: Efficiency versus True Air Speed.

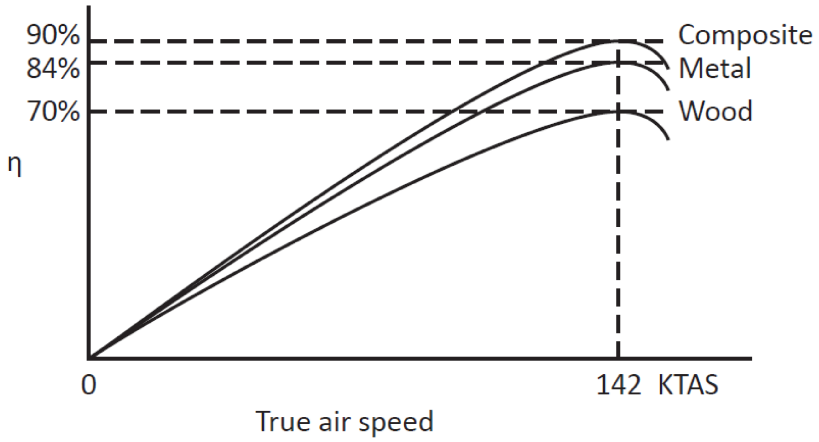


Source: Hitchens [7]

# 4 Blade Element Momentum Theory

Glauert's analysis, as presented in [5], delves into the equations governing propeller performance. This model combines unidimensional momentum theory with blade element theory. The former approximates airscrews as very thin discs interacting with airflow to exchange energy, while the latter considers the number of blades and their shapes to compute the balance of forces in the rotor.

$$dT = C_T \frac{1}{2} \rho V_x^2 dA \tag{12}$$

$$dQ = C_Q \frac{1}{2} \rho V_x^2 dA r \tag{13}$$

To compute the forces involved, the airscrew disk is divided into infinitesimally small annular sections with radius $dr$. For these annuli, the area $dA$ can be approximated as $rdr$. Consequently, $dT$ and $dQ$ represent thrust and torque, respectively. Each annulus is associated with thrust and torque coefficients, denoted as $C_T$ and $C_Q$. These coefficients are directly linked to the acceleration experienced by the fluid as it passes through the disk.

The acceleration is considered through the definition of interference parameters: $a_x$, representing axial acceleration, and $a_y$, associated with the rotational motion imparted to the fluid. These parameters are integral to equations 14 and 15, alongside $F$, a parameter capturing energy losses due to the formation of vortices.

$$C_T = 4F a_x (1 + a_x) \tag{14}$$

$$C_Q = 4F a_y (1 + a_x) \frac{V_y}{V_x} \tag{15}$$

As it was mentioned, the blade element theory uses airfoil polars, which in the tool developed are obtained as described further. However, in equations 16 and 17, $B$ stands for the number of blades, so it can be written:

$$dT = B C_x \frac{1}{2} \rho W^2 c dr \tag{16}$$

$$dQ = B C_y \frac{1}{2} \rho W^2 c r dr \tag{17}$$

The airscrew, also, is divided radially into stations to calculate the forces that appear. But, $C_T$ and $C_Q$ are calculated differently as they are a function of the plan form of the blade section, and relative airflow, which is represented by $W$ [13]. By decomposing the forces in Image 13, the forces in the blade section are presented in Figure 22 below.

Figure 22: Forces in blade section.

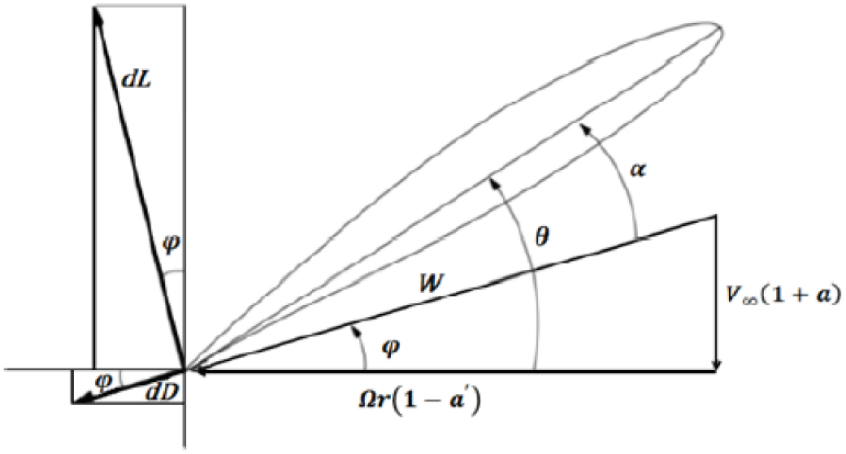


Source: Tarraran [13]

$$W = \sqrt{(V_x(1+a_x))^2 + (V_y(1-a_y))^2} \tag{18}$$

But in this case:

$$\begin{bmatrix} C_x \\ C_y \end{bmatrix} = \begin{bmatrix} cos\theta & -sin\theta \\ sin\theta & cos\theta \end{bmatrix} \begin{bmatrix} C_l \\ C_d \end{bmatrix} \tag{19}$$

In these Equations, $C_l$ and $C_d$ denote lift and drag coefficients, while $C_x$ and $C_y$ signify force coefficients in the axial and tangential directions. By setting the quantities $dT$ and $dQ$ obtained from different theories equal to each other, these equations yield the following interlinked solution. Here, $\theta$ represents the inflow angle, delineating the difference between local $\beta$ and $\alpha$ and establishing the direction of the local airstream.

$$a_z = \frac{C_x\sigma}{4Fsin^2\theta + C_x\sigma} \tag{20}$$

$$a_y = \frac{C_y\sigma}{4Fsin^2\theta + C_y\sigma} \tag{21}$$

Upon determining the values of the interference parameters, the remaining parameters involved in the preceding equations can be derived. This model serves to assess propeller performance, and the resolution of the aforementioned equations is explored in Section 4.3. In this section, a comparison is made between the methods proposed by Adkins [2] and Ning [11].

Upon solving BEMT equations and obtaining the values of $C_x$ and $C_y$, thrust and torque per station are calculated using Equations 16 and 17. Subsequently, the total thrust and torque are determined by summing the contributions from each section into which the blade is divided. This summation is performed through a trapezoidal approximation, where the subscripts $i$ and $i+1$ correspond to their respective stations, and $r$ denotes the axial position of the station:

$$T = \sum_{i=1}^{n-1} \frac{dT_i + dT_{i+1}}{2} r_{i+1} - r_i \tag{22}$$

$$Q = \sum_{i=1}^{n-1} \frac{dQ_i + dQ_{i+1}}{2} r_{i+1} - r_i \tag{23}$$

As Section 3 explained the efficiency, other non-dimensional quantities that help compare propeller performance are now defined in equations from 24 to 27:

$$J = \frac{V}{n_s d} \tag{24}$$

$$C_T = \frac{T}{\rho n_s^2 d^4} \tag{25}$$

$$C_Q = \frac{Q}{\rho n_s^2 d^5} \tag{26}$$

$$C_Q = \frac{Q}{\rho n_s^3 d^5} \tag{27}$$

Parameter $J$ is called advance ratio and is used when operating conditions of a propeller are defined, $n_s$ is the number of stations, so that propeller performance $C_T$ and $C_Q$ $C_P$ and $\eta$, can be recalled.

## 4.1 Model parameters

### 4.1.1 Geometry

The list of propeller geometry parameters is:

- Number of blades ($B$);
- Diameter ($d$);
- Cut-off ratio ($R_{Cut-off}$);
- Distribution of stations along the blade ($\xi(r)$);
- Chord and twist distribution ($e(\xi(r))$) and ($\beta(\xi(r))$);
- Number of stations($n$).

As there are functions of the distance from the axis rotation and twist and chord distribution, it can be figured out with a correlation with the distributions of stations along the blade span. These parameters are implemented as vectors, with the current position assigned.

The parameters mentioned earlier are sufficient for characterizing propeller geometry. However, there are additional parameters that can be derived from them and play a crucial role in the Blade Element Momentum Theory (BEMT) equations. One such parameter is the blade solidity, which appears in Equations 37 and 38. Blade solidity is defined as the ratio of the total blade area to the area of the circular disc swept by the blades.

$$\sigma = \frac{Bc}{2\pi r} \tag{28}$$

If the airscrew's movement resembled that of a screw in a rigid medium, each section would move forward by a distance of $2\pi r \tan \beta$. This displacement, termed $H$, is known as the geometrical pitch of the propeller. A propeller with a twist distribution following the law in Equation 6 is classified as having a constant geometric pitch. While the geometrical pitch lacks aerodynamic significance, the $H/d$ ratio proves valuable for propeller classification. Figure 23 illustrates efficiency vs. advance ratio curves for a propeller family across various $H/d$ ratio values.

Figure 23: Efficiencies of a propeller family.

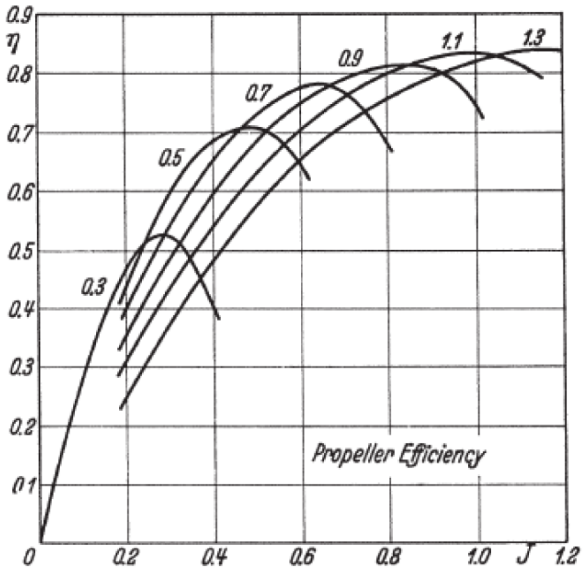


Source: Glauert [5]

### 4.1.2 Air conditions

Also, other fundamental variables to discuss is the fluid that surrounds the propeller:

- Forward speed of the aircraft ($V$);
- Rotational speed ($\Omega$ or $n_s$);
- Density ($\rho$);
- Speed of sound ($V_s$);
- Airflow speed ($V_\infty$).

Forward speed minus airflow speed and rotational speed module result in local flow speed, as in Figure 22. The tool works with the module of these speeds and is easily implemented as they are scalar parameters. Density and temperature that depend on the phase of the aircraft mission are needed to compute Reynolds and Mach numbers, numbers that lift and drag coefficients are functions of.

### 4.1.3 Database and aerodynamics

The BEMT is based on knowing the lift and drag coefficients of the section, which are a function of Reynolds and Mach numbers, angle of attack, and airfoil of the section. Two main issues appear when trying to write a code that solves the BEMT equations, which are: how to obtain airfoil characteristics and when the routine needs them. Starting with the latter, it is clear that, the process of solving BEMT equations affects the times in which the user needs to provide lift and drag coefficients as an input, and depending on the routine, this number of times varies.

There are two possibilities to get lift and drag coefficients, one is calculating them directly by an implementation of any existing method and the other is to call other routines that calculate aerodynamic coefficients only when it is needed to. XFOIL is an interactive program for the design and analysis of subsonic isolated airfoils [4]. Developed by Professor Mark Drela and released under the GNU General Public License, can be used to obtain the aerodynamic information searched. Therefore it is possible to call XFOIL during the resolution of the BEMT equations or write a program that automatizes the creation of a database of polar curves for different Reynolds and Mach numbers. This database is created prior to the start of the calculations and retrieved during program execution. It's important to notice that XFOIL, the software used to construct the database considers the air an incompressible fluid.

Figure 24: XFOIL processing to build the database.

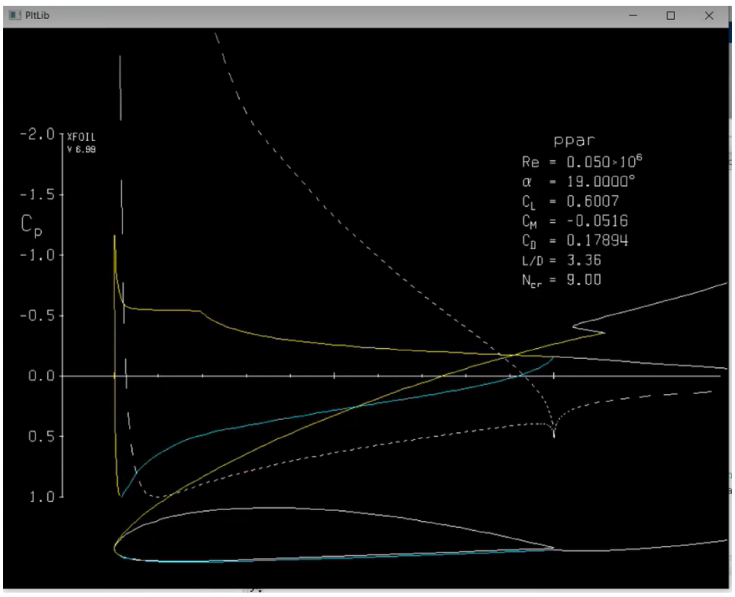


Source: Own Authorship.

Calling XFOIL between iterations to obtain direct lift and drag coefficients is very flexible. Also, if necessary, it could allow a parametrization of airfoil geometry to include

this parametrization as a variable during propeller geometry optimization. However, this would be very time-consuming. Then, an approach utilizing an already saved polar for each airfoil is utilized and such parametrization wouldn't be considered.

Preparing a polar database presents new difficulties. XFOIL is designed to provide subsonic data and, for high subsonic Mach numbers, it is inaccurate. Therefore, other sources of aerodynamic data must be considered to compensate for the absence of this data. So, to extrapolate data for angles of attack higher than that of the stall, the Viterna method[14] is explained in Subsection 4.2.

Martin [10] in his thesis, he presents a Harris [6] study. It presents data for the NACA 0012 symmetric airfoil at high subsonic Mach numbers, gathered from wind tunnel experiments, is provided. An example of this data is displayed in Figure 25. On the other hand, implementing this data for just one airfoil wouldn't contribute this much to the objective of this thesis. For higher Mach conditions, it was considered the same as the highest value extracted from XFOIL, 0.5.

Figure 25: $C_L$ and $C_D$ of NACA 0012 M = 0.76.

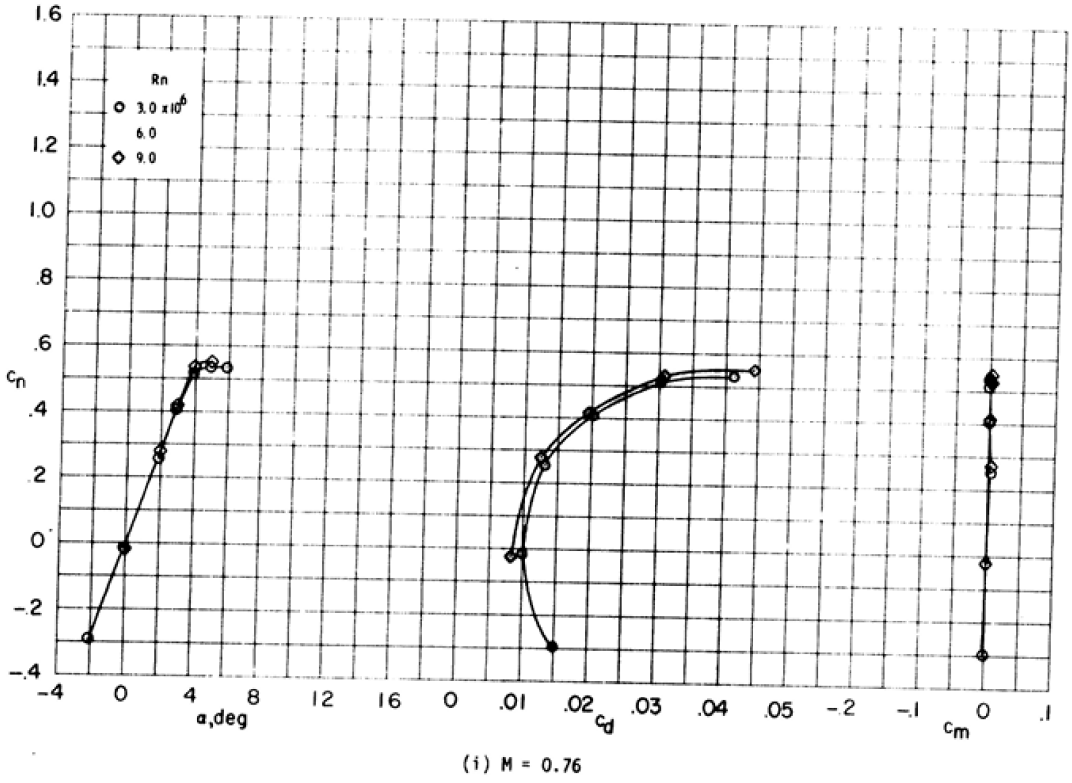


Source: Harris [6]

XFOIL allows exporting the database calculated as text files, and later opened by other computer programs. MATLAB can save the data in files *.mat*. This format is simple to understand and since it is an own MATLAB file, it doesn't require computational time to read the data. Therefore, this type of format was chosen to compose the database.

The matfiles in the database are composed of columns of data on the lift and drag coefficients as a function of the angle of attack. Every text file contains these values for a couple of Reynolds and Mach values. Martin [10], in his master's degree thesis separated for every airfoil, the Reynolds and Mach numbers of which the database is made, take

discrete values from $5.10^4$ up to $5.10^6$ in steps of $5.10^4$ and 0 up to 0.5 in steps of 0.05 respectively. So, this thesis also utilizes this step, because it was considered a good spacing.

During the database construction, XFOIL showed some miscalculation in converging its results. XFOIL uses an interaction method to calculate the interaction of fluid with panels. However, when the interaction doesn't converge, the program doesn't save the result, as you can see on Figure 26 some blank spaces.

Figure 26: Polynomial generated by CLARK Y in $Re = 50000$ and $Mach = 0.35$.

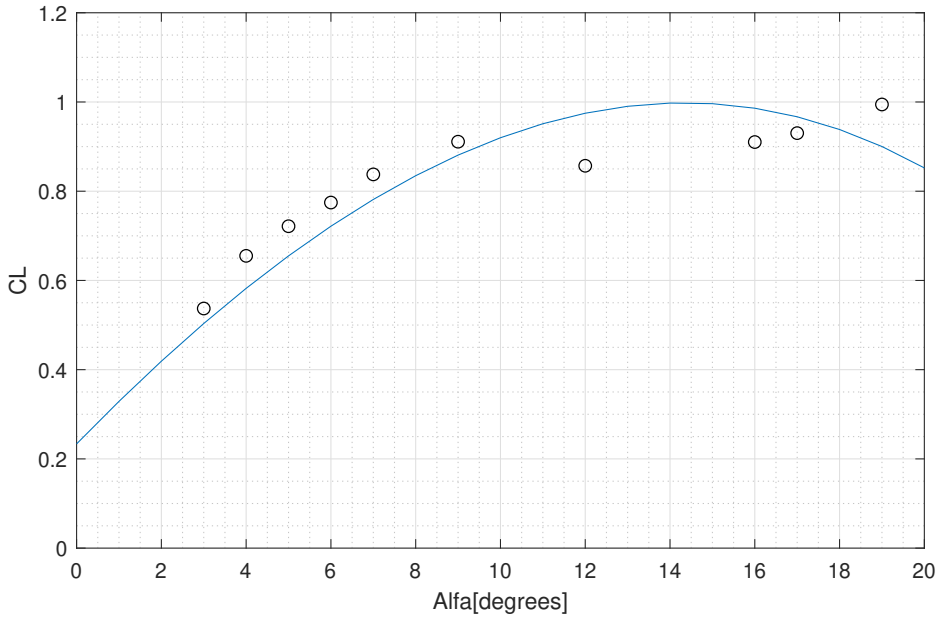


Source: Own authorship.

To solve this issue, the creation of codes to read and fix the files were created. They read the files, and checked the number of rows, if they had a low quantity of rows, the code acquired data again from XFOIL, but with a little change in Reynolds number.

Therefore, a polynomial was created by four sets of data collected in the files that contain the closest Reynolds and Mach numbers exemplified by Figure 26. Then, these polynomials were interpolated to define the specific coefficient of lift and drag exemplified by Figure 27.

Figure 27: Example of specific $Alpha = 18.9$.

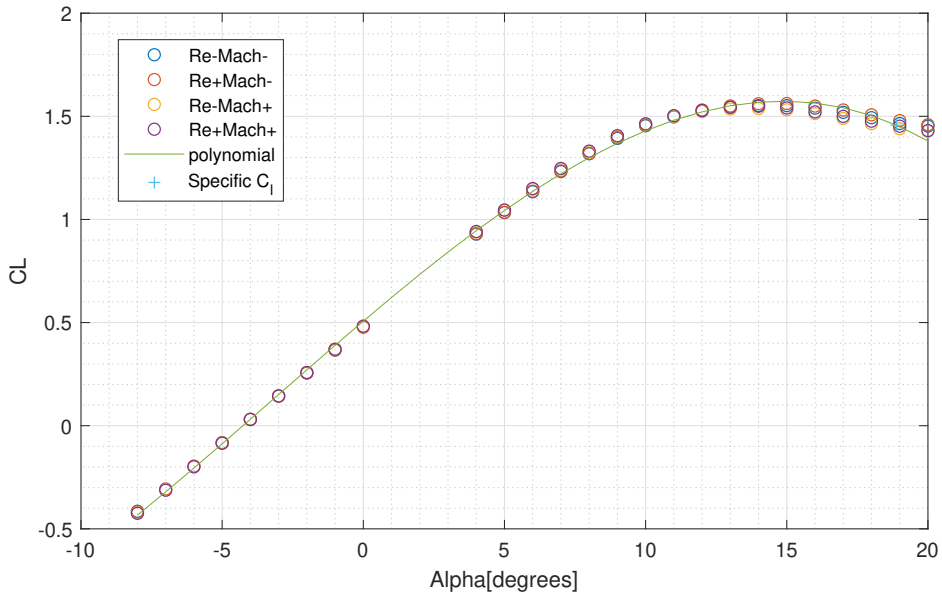


Source: Own authorship.

## 4.2 Viterna extrapolation

Viterna extrapolation, also known as the Viterna method, is a technique used in aerodynamics to estimate the performance of an airscrew at high wind speeds. As it's designed to operate optimally within a specific range of wind speeds, during extreme weather conditions or gusty winds, the wind speed can exceed the turbine's designed limit.

The Viterna extrapolation method helps predict how an airscrew will perform beyond its rated wind speed by using a combination of experimental data and mathematical modeling. It is particularly useful in estimating the propeller's power output and loads on components when operating in high-speed wind conditions. This situation can appear for several reasons: low horizontal speed versus rotational speed ratio, high pitch of the blade, etcetera.

The following equations are based on Viterna [14] and [8]. This method takes into account the stall angle of attack and lift coefficient, maximum drag coefficient, and aspect ratio of the blade to provide this consideration.

$$C_D = B_1 sin^2\alpha + B_2 cos^2\alpha \tag{29}$$

$$C_L = A_1 sin2\alpha + A_2 \frac{cos^2\alpha}{sin\alpha} \tag{30}$$

As these variables ($A_1$, $A_2$, $B_1$, and $B_2$) will be defined with a loop till converge these equations, $C_L$ and $C_D$ must be known to facilitate the iteration. In this case, these variables are proportional as shown in the Equations below.

$$A_1 = B_1/2 \tag{31}$$

$$A_2 = (C_{L_S} - C_{D_M} sin\alpha_s cos\alpha_s)\frac{sin\alpha_s}{cos^2\alpha_s} \tag{32}$$

$$B_1 = C_{D_M} \tag{33}$$

$$B_2 = (C_{L_S} - C_{D_M})\frac{sin^2\alpha_s}{cos\alpha_s} \tag{34}$$

- Lift at stall angle of attack ($C_{L_S}$);
- Drag at stall angle of attack ($C_{D_M}$);
- Stall angle of attack ($\alpha_s$);

Since stall angle is defined by Anderson [3] as the angle when the lift reaches the highest value, it's possible to define these coefficients after defining a correlation of $\alpha x C_L$.

## 4.3 BEMT Interation

Tarraran [13] used an iterative method similar to the one used in this analysis that is shown in the flow chart on Image 28.

Starting with the provided chord and twist distributions, the number of blades, the airfoil section, and the propeller diameter, an initial estimation is used for the parameter $\phi$. Figure 22 illustrates the connection between the inflow angle, angle of attack, and local twist angle. Using this relationship, the angle of attack is determined using the initial estimation and the known twist distribution. The angle of attack, along with the Reynolds and Mach numbers, allows for the computation of lift and drag coefficients. Subsequently, $C_x$ and $C_y$ are calculated based on the chord and twist distribution. The process then proceeds to calculate the Goldstein loss factors $K$ and $K'$ as follows:

$$K = \frac{C_y}{4sin^2\phi} \tag{35}$$

$$K' = \frac{C_x}{4cos\phi sin\phi} \tag{36}$$

These two factors are crucial parameters that consider losses and facilitate the adjustment of BEMT equations in the quest for the desired solution. With the help of these factors, it becomes feasible to compute the interference factors, denoted as $a_x$ and $a_y$, as follows:

$$a_x = \frac{\sigma K}{F - \sigma K} \tag{37}$$

$$a_y = \frac{\sigma K'}{F - \sigma K'} \tag{38}$$

Figure 28: BEMT equations calculation algorithm.

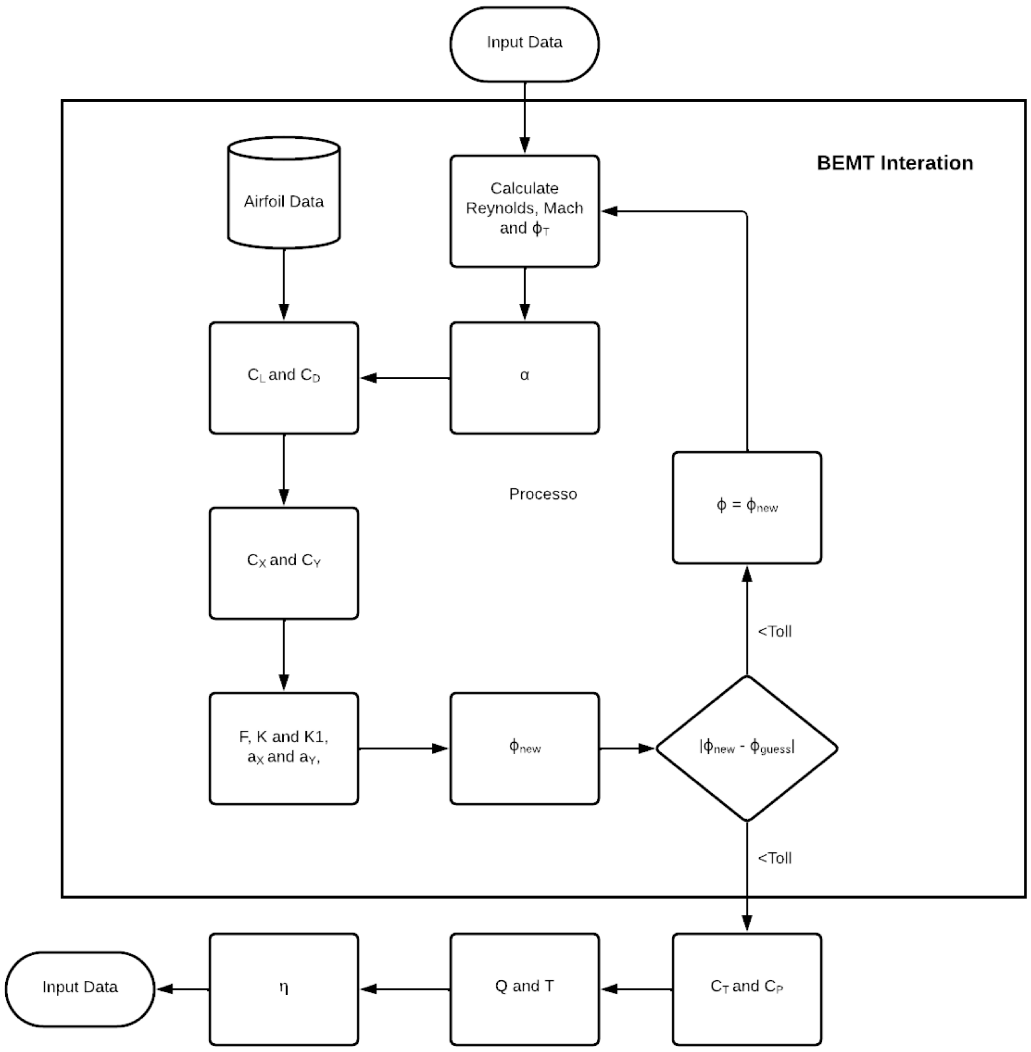


Source: Own authorship.

The Prandtl factor $F_P$, which accounts for tip losses, is determined using the following expression. The variable $f$ is defined as follows, with $\phi_t$ representing the inflow angle at the tip.

$$F_P = \frac{2}{\pi} \arccos e^{-f} \tag{39}$$

$$f = \frac{B}{2}(1 - \xi)/\sin\phi_t \tag{40}$$

As the BEMT equations are solved individually for each station, the determination of the inflow angle at the tip adheres to the requirement that the vortex sheet in the wake forms a rigid helical surface. This condition is achieved through the use of the following equation:

$$\tan\phi_t = \frac{B}{2}(1 - \xi)/\sin\phi_t \tag{41}$$

Lastly, with the updated interference factors in hand, considering the speed triangle formed by the axial speed ($V$) and rotational speed ($\Omega$) that have been adjusted by the interference factors depicted in Figure 22, we can calculate the new orientation of the local airstream. This new inflow angle value is obtained using the following equation:

$$\phi_{new} = \arctan \frac{V(1 + a_x)}{r\Omega(1 - a_y)} \tag{42}$$

This updated angle $\phi$ is then compared to the value associated with the current iteration. If the difference exceeds the acceptable error threshold, the inflow angle value is adjusted, and the algorithm recommences its calculations until $\phi$ converges. At this stage, all the required variables have been computed, allowing for the determination of the propeller's performance, as elaborated in Subsection 4.1. It's worth noting that this algorithm might halt before reaching convergence, especially because the calculations become increasingly sensitive once the Prandtl loss factor is computed (as indicated in Equation 39).

While the approach introduced by Ning in [11] is suitable for resolving Blade Element Momentum Theory (BEMT) equations, it establishes the possibility of always discovering a solution for Equation 43. Notably, this equation exclusively relies on the inflow angle $\phi$. Given a fixed propeller geometry ($\sigma$), along with specified flight conditions involving horizontal speed ($V_x$) and rotational speed ($V_y$ at the station), and, of course, having a database of polar data prepared, the primary objective is to determine the value of $\phi$ that serves as the solution to this equation.

$$V_y(4F\sin^2\phi - C_x\sigma) - V_x(2F\sin 2\phi + C_y\sigma) = 0 \tag{43}$$

# 5 Accelerated Differential Evolution

Martins [9] introduces optimization as a human instinct, in biology, it's exemplified as the evolution of species. Mathematically it's a much more precise concept, the best possible solution may be found by changing the variables that affect the result.

While some simple problems can be solved analytically, many cases are too complex to solve this way. The advent of computational evolution allowed the development of high-level optimization algorithms. So, many methodologies were created to find these better results in less time.

Figure 29: Example of engineering machine learning algorithms.

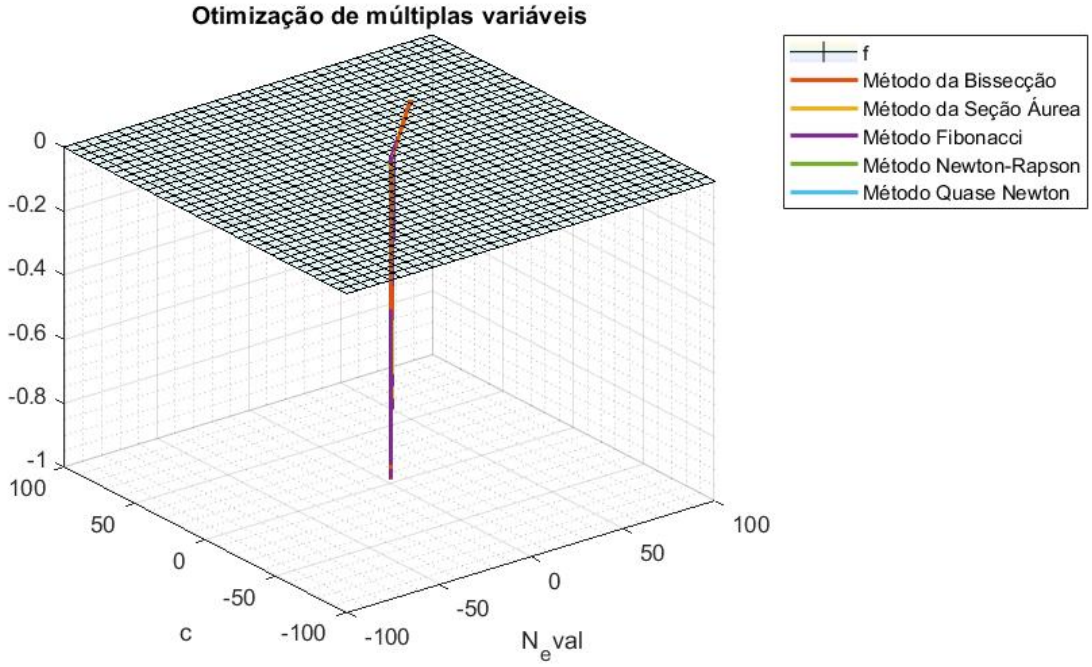


Source: Own Authorship.

A large segment of applications focuses on the design of engineering systems. Optimization of propeller geometry showed a dependence on some variables that only a complex method could define an optimum result.

Figure 30 demonstrates the flow chart to formulate an optimization process. This document describes all the criteria imposed further. The constraints can be improved since XFOIL doesn't have precise results for high Mach, as it considers incompressible fluid, however, the output is considered close to real.

Figure 30: Optimization problem formulation steps.

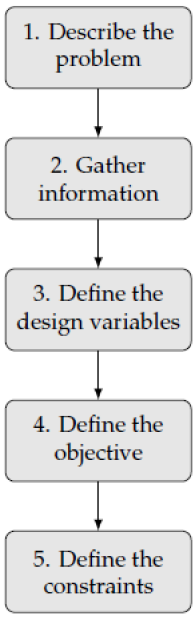


Source: Martins[9]

## 5.1 Genetic Algorithms

Genetic algorithms (GAs) are the most well-known and widely used type of evolutionary algorithm. This type of method defines individuals with a set of variables (chromosomes), in the population, the individuals are selected, and the chromosomes suffer crossover and mutate, based on natural selection(evaluation). It allows the members of the population to acquire favorable adaptations to survive longer and contribute more to the population goal.

Differential evolution (DE) is a method that optimizes a problem by iteratively trying to improve a candidate solution concerning a given measure of quality. Such methods are commonly known as metaheuristics as they make few or no assumptions about the optimized problem and can search very large spaces of candidate solutions. However, metaheuristics such as DE do not guarantee an optimal solution is ever found.

Accelerated Differential Evolution (ADE) is a GA refers to enhancements and modifications made to the basic DE algorithm to improve its convergence speed and solution quality. These enhancements include:

- Advanced Mutation Strategies: Using more sophisticated mutation strategies that adapt to the problem's characteristics. This could involve techniques like self-adaptive scaling factors or different mutation strategies for different individuals;
- Adaptive Control Parameters: Dynamically adjusting algorithm parameters (such as mutation and crossover rates) as the optimization progresses to fine-tune the search process;
- Local Search Techniques: Incorporating local search methods to explore the solution space around promising individuals in a more focused manner, potentially increasing exploitation capabilities;

- Population Diversity Maintenance: Strategies to maintain diversity within the population, such as crowding or niching techniques, to prevent premature convergence to suboptimal solutions;
- Parallelization: Utilizing parallel computing to evaluate multiple candidate solutions simultaneously, which can speed up the optimization process;
- Hybrid Approaches: Combining Accelerated Differential Evolution with other optimization techniques or problem-specific heuristics to leverage their strengths.

The term "Accelerated" implies that these enhancements and modifications aim to make the optimization process more efficient and effective, allowing the algorithm to find better solutions in a shorter amount of time compared to the basic Differential Evolution(DE) algorithm. However, the specific techniques used in ADE may vary based on the problem at hand and the research advancements in the field.

So, ADE presents an optimum approach to start the process of defining the best propeller for a specific engine. Due to its fast designing approach to favorable results, it can be used for the project conceptual stage, succeeded by Computational Fluid Dynamics(CFD) in the other stages, to optimize even more the airscrew.

Figure 31: ADE application in BEMT.

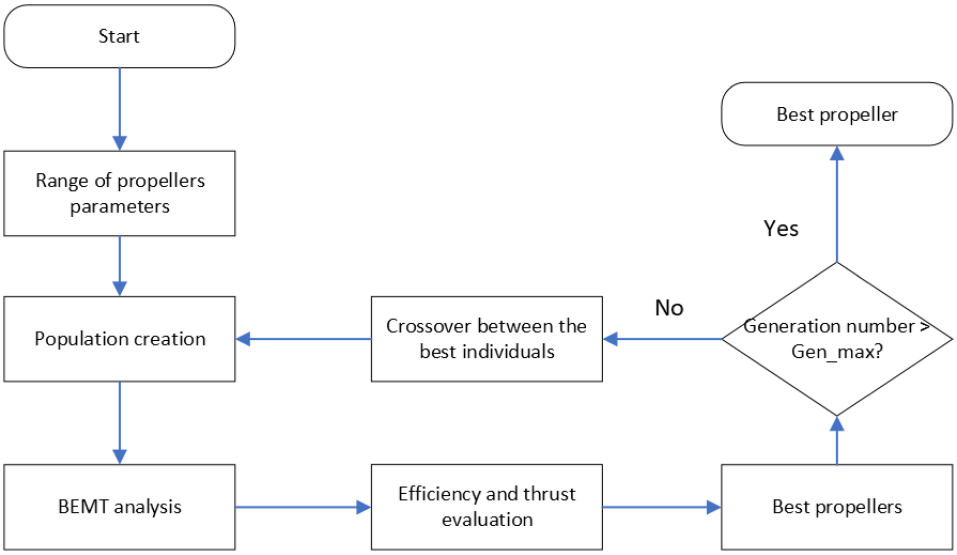


Source: Own authorship.

## 5.2 BEMT Aplication

First, the design variables are the propeller parameters, which include number of blades, blade radius, section quantity, airfoil, inflow angle, twist angle, and chord. Also, the conditions are necessary, the $\Omega$ and $Torque$, as these conditions depend on the engine, which has the optimum operating condition, the rotation per minute was established as constant, and the $Torque$ is penalized if it's higher than the maximum condition defined.

Since the twist and chord can be seen as a second-degree polynomial, shown in Figure 32. These parameters are calculated as a section position function. Based on Adkins'

propeller[2], the inflow angle can be defined as a first-degree polynomial added to the value of twist angle, also as a section function.

$$c = c_A x^2 + c_B x + c_C \tag{44}$$

$$\mathrm{B} = \mathrm{B}_A x^2 + \mathrm{B}_B x + \mathrm{B}_C \tag{45}$$

$$\phi = \mathrm{B}_A x^2 + [\mathrm{B}_B + \phi_A] x + \mathrm{B}_C + \phi_B \tag{46}$$

Other assumptions were made: For a construction and structural limit, the chord section was stipulated to not be less than 0.04 meters. Also, the blade can't have more than two airfoils, due to the complexity of the construction.

# 6 Validation

## 6.1 Analytical validation

Using Ning's approach to resolve BEMT equations the performance of a propeller that helped as an example in [2] was obtained. Adkins provides an example of the use of the algorithm described in its article. The propeller was designed to work at 110 mph (49m/s) and 2400 rpm. The airfoil of the section is the NACA 4415 and is maintained constant along the span. An extract of the article in which the geometry is defined is present in Table 1.

Table 1: Adkins' propeller parameters

| r [mm] | c [mm] | $\beta$ [deg] | $\phi$ [deg] |
|---|---|---|---|
| 152.4 | 104.3 | 58.3 | 54.8 |
| 273.0 | 140.3 | 41.8 | 38.3 |
| 393.7 | 130.1 | 32.2 | 28.7 |
| 514.3 | 108.7 | 22.2 | 22.7 |
| 634.9 | 85.2 | 18.7 | 18.7 |
| 755.6 | 58.3 | 15.9 | 15.9 |
| 876.3 | 0.0 | 13.8 | 13.3 |

Figure 32: Adkins propeller geometry.

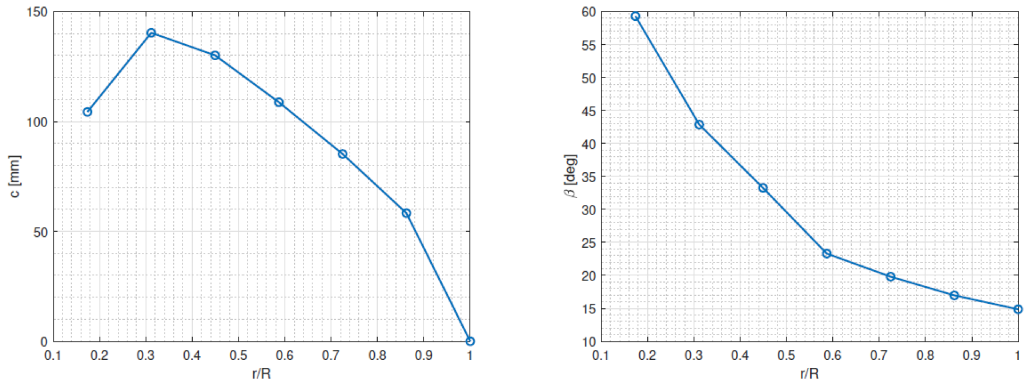


(a) *Chord distribution* (b) *Twist distribution*

Source: Adkins [2]

For this propeller, its performance was calculated and confronted with the results achieved in the Adkins[2]. First, Figure 33 represents the global thrust and torque generated by the propeller. Figures 34, 35 and 37 display two curves, those in red are obtained with the tool developed, and in black is the data present in the article, while an asterisk marks the design point for which the propeller was designed. Figure 36 does not provide information about the required torque coefficient obtained through the Adkins algorithm as there was no data provided.

Figure 33: Thrust and Torque Adkin's propeller results from BEMT.

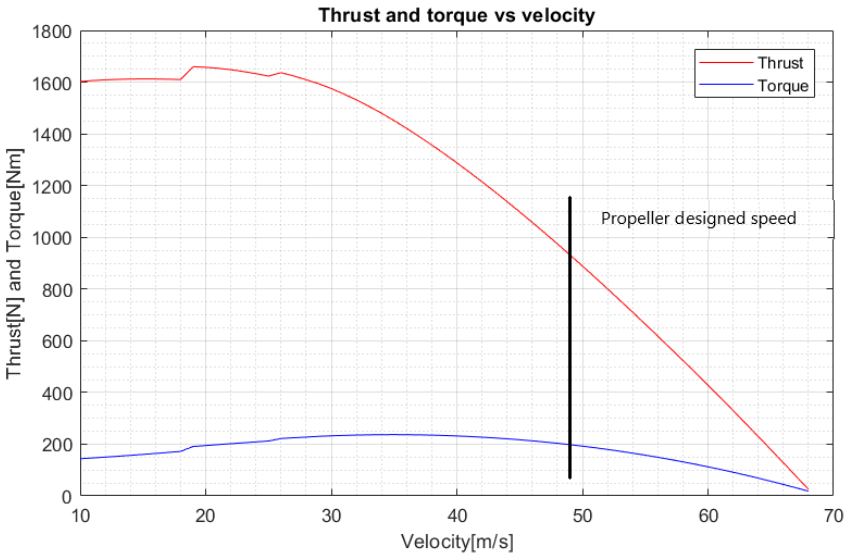


Source: Own authorship.

Figure 34: Adkin's propeller efficiency comparison of results.

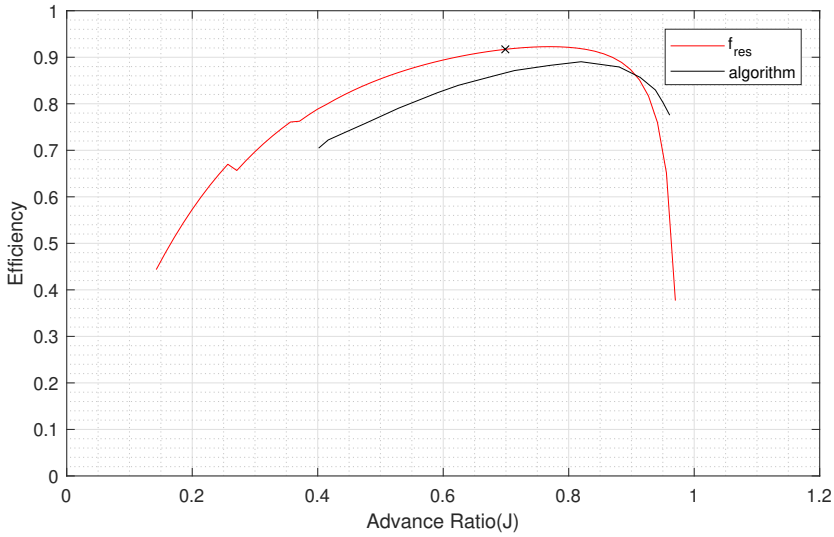


Source: Own authorship.

Figure 35: Adkin's propeller thrust coefficient comparison of results.

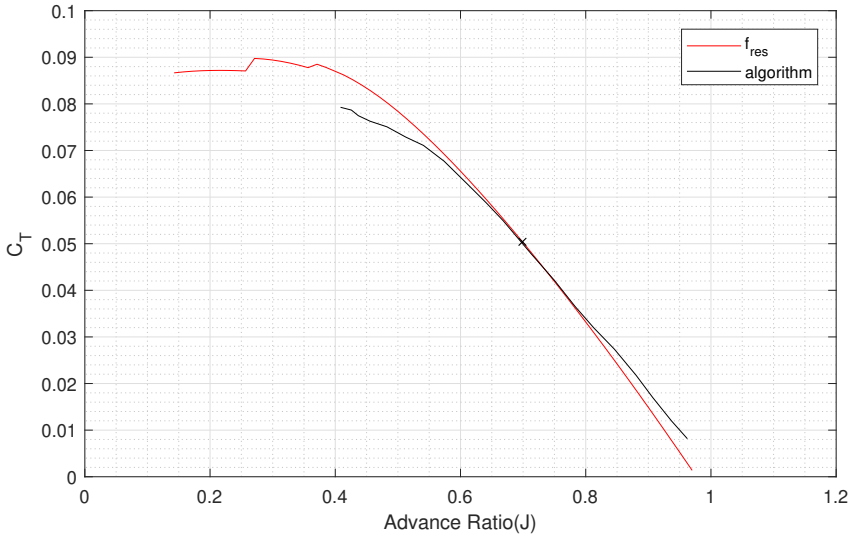


Source: Own authorship.

Figure 36: Adkin's propeller torque coefficient BEMT results.

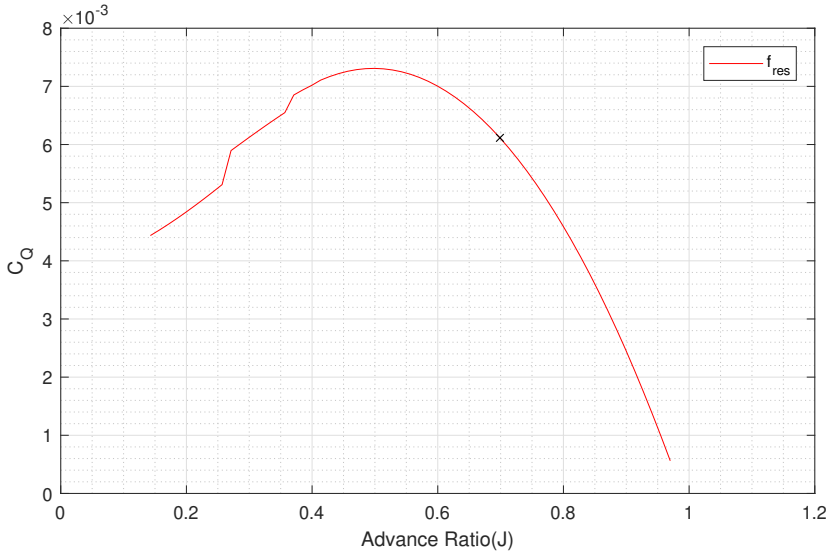


Source: Own authorship.

Figure 37: Adkin's propeller power coefficient comparison of results.

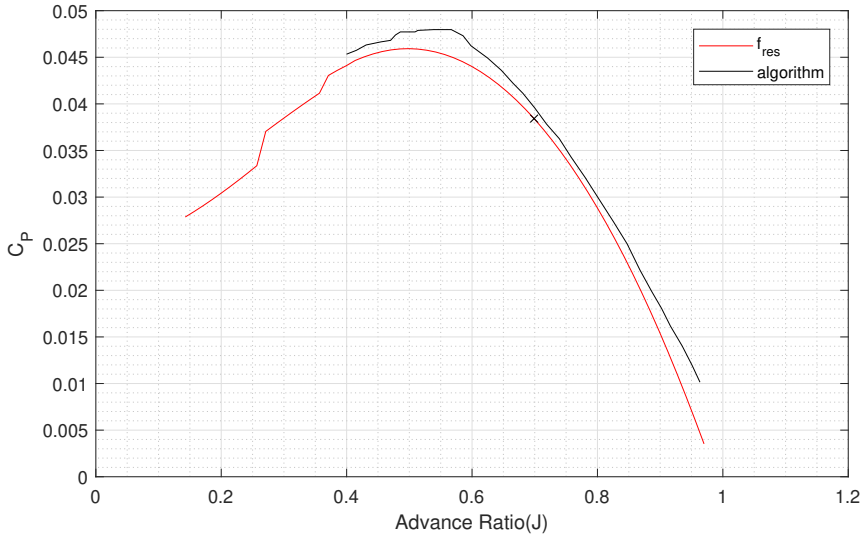


Source: Own authorship.

It's possible to state with Figure 34 that the results were similar to the ones presented by Adkins. The small deviation were calculated and presented in the Table 2.

Adkins' algorithm's credibility was established in the article [2] through favorable comparisons with real propeller performance data obtained from experiments. Since the algorithm appears to yield consistent results with validated data, it is reasonable to perform another confrontation with real propeller performance.

Table 2: Efficiency error compared to the Adkins' result

| J | Error |
|---|---|
| 0.4 | 11.96% |
| 0.5 | 10.32% |
| 0.6 | 7.83% |
| 0.7 | 5.74% |
| 0.8 | 3.37% |
| 0.9 | 1.15% |

## 6.2 Experimental validation

The approach introduced by Martín[10] demonstrated a strong agreement with Adkins' method for the assessment of propeller performance. This alignment is particularly encouraging, as Adkins' algorithm's credibility was established in the article[2] through favorable comparisons with real propeller performance data obtained from experiments. However, given that the algorithm appears to yield results consistent with validated data, and considering the similarities between the calculations conducted using the developed tool and the algorithm, it is reasonable to perform another confrontation with real propeller performance.

Table 3: Xiang's propeller parameters

| r [mm] | c [mm] | $\beta$ [deg] | $\phi$ [deg] |
|---|---|---|---|
| 60.0 | 128.2 | 66.0 | 62.0 |
| 134.0 | 141.7 | 57.9 | 53.9 |
| 245.0 | 149.8 | 40.6 | 36.6 |
| 356.0 | 141.9 | 31.4 | 28.4 |
| 467.0 | 119.6 | 26.1 | 20.1 |
| 578.0 | 90.2 | 21.8 | 18.8 |
| 689.0 | 60.7 | 17.5 | 14.5 |
| 800.0 | 0.0 | 16.0 | 13.0 |

Xiang et a[15] research studies a propeller with the parameters in Table 3 and RAF 6. The experiment results are displayed in Figures 38 to 42. Also, their document shows another method to analyze the propeller performance that won't be discussed in this thesis, however, with more experimental results of different propellers, BEMT and the method proposed could be compared to define the best approach.

Figure 38: Thrust and Torque results from BEMT.

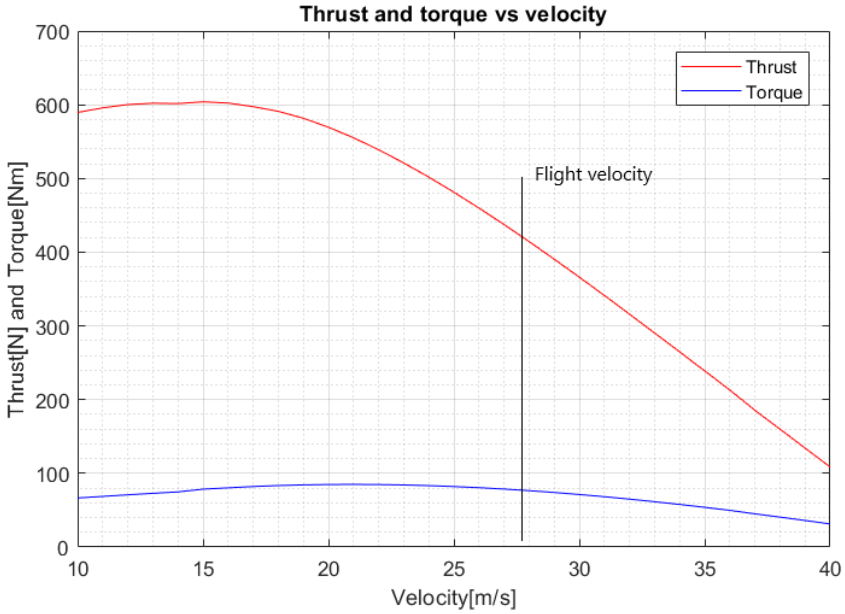


Source: Own authorship.

Figure 39: Efficiency comparison of test results and numerical BEMT results.

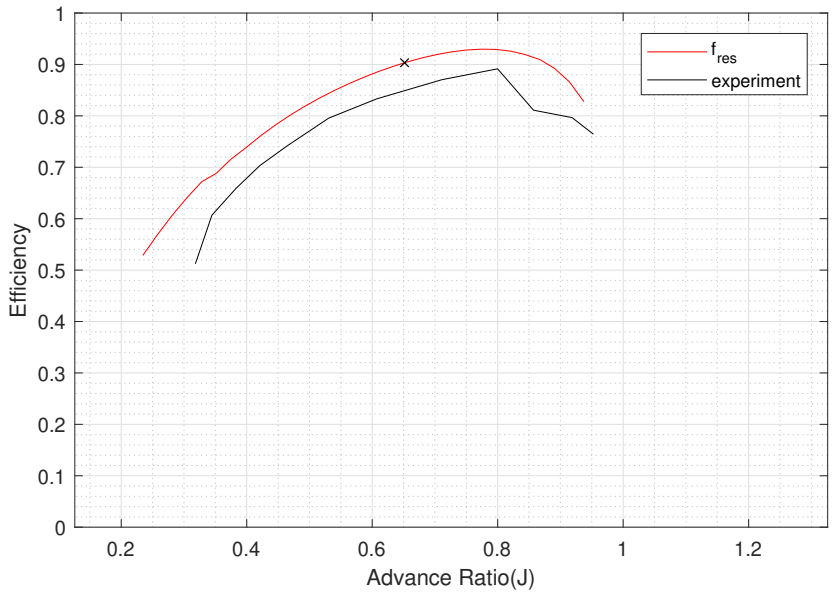


Source: Own authorship.

Figure 40: Thrust coefficient comparison of test results and numerical BEMT results.

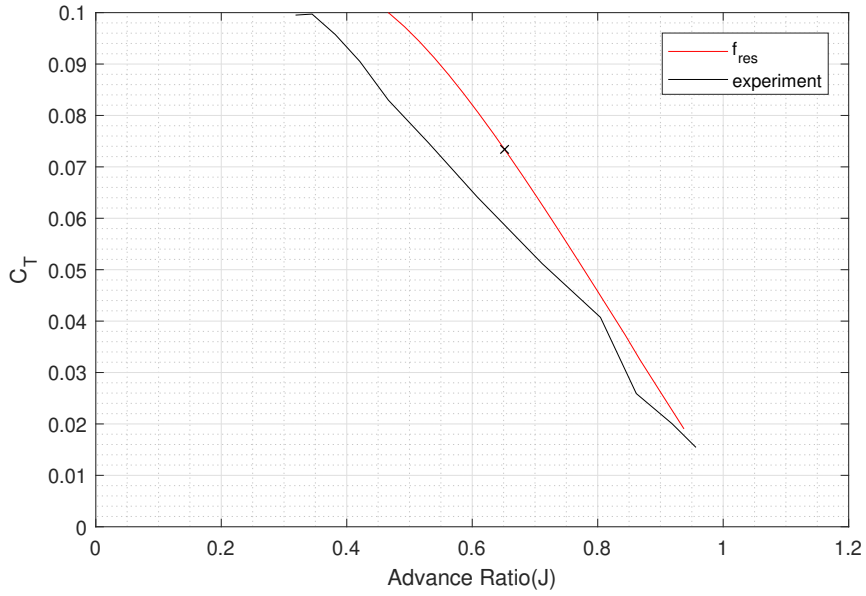


Source: Own authorship.

Figure 41: Torque coefficient comparison of test results and numerical BEMT results.

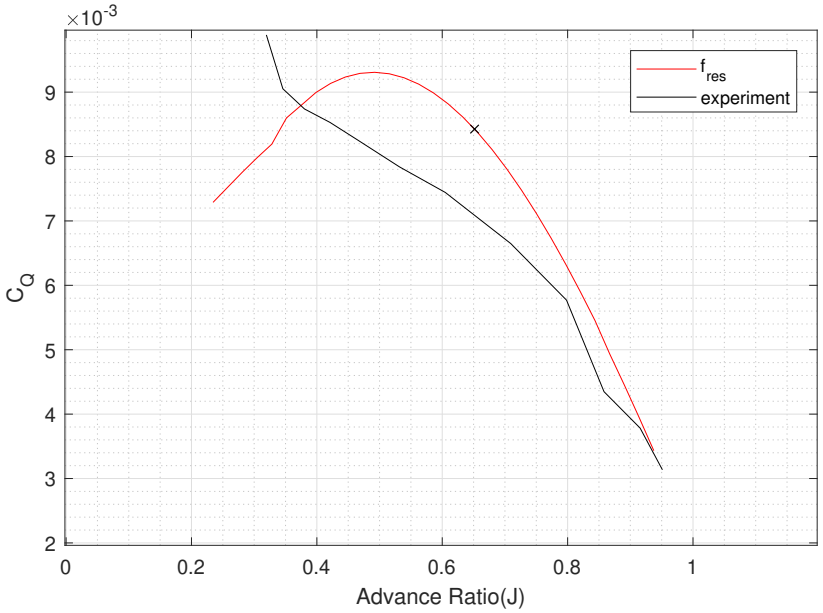


Source: Own authorship.

Figure 42: Power coefficient comparison of test results and numerical BEMT results.

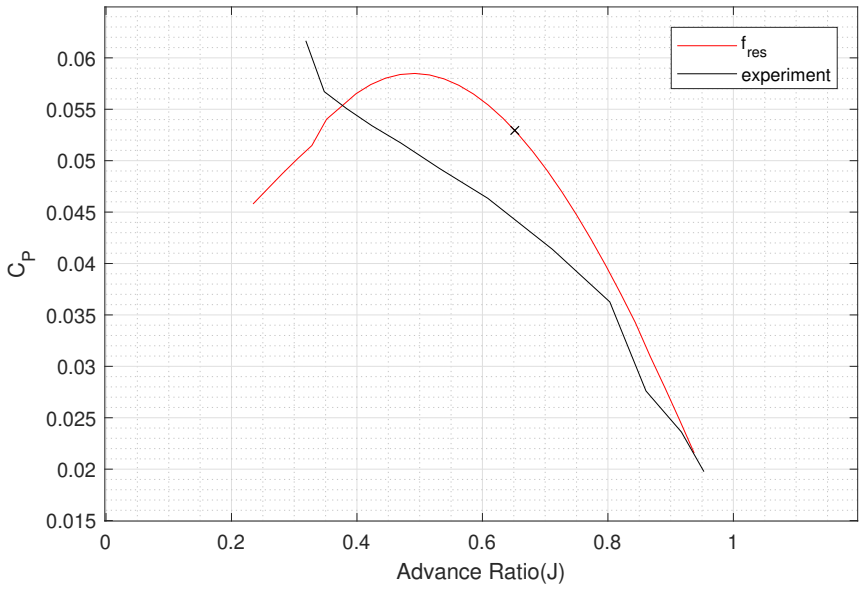


Source: Own authorship.

In the comparison of the black curves with the red ones, a deviation presented in Table 4 is noticed. It is noticeable that discrepancies occur in all the ranges of the Advance Ratio. Since the RAF 6 database was the most inconsistent, it wasn't possible to define the reason for this error. Taking into consideration the deviation, it still brought reliable results.

Table 4: Efficiency error compared to the Xiang' result

| J | Error |
|---|---|
| 0.4 | 8.37% |
| 0.5 | 6.43% |
| 0.6 | 6.36% |
| 0.7 | 5.64% |
| 0.8 | 4.23% |
| 0.9 | 5.60% |

Also, another comparison was made, the results between the Martín[10] algorithm and the one proposed in this thesis. Overall, there is a good correlation between the computations of the two calculating methods presented in this section.

# 7 Results

## 7.1 ADE Results

The ADE results are divided into three stages based on the convergence or divergence of setup parameters. The first stage probably is devoted to understanding the ADE interaction with BEMT. The second is a prior analysis to understand the convergence of parameters, and the third is the final definition of the set up of limits to define the best propeller for the case proposed.

### 7.1.1 First Stage

To introduce, the first ADE BEMT analysis involved a setup of a high range of limits from some parameters, while small to others. The main idea of this phase, as mentioned above, is to study this method and not make any hasty conclusions. First, the polynomial coefficients were obtained from Adkins' propeller. Later, set up a small margin for these three variables. The limits and the results are shown in Table 5.

Table 5: First stage ADE iteration results

| Parameters | Inferior limit | Superior limit | Iter 1 | Iter 2 | Iter 3 |
|---|---|---|---|---|---|
| $B$ | 2 | 5 | 5 | 4 | 4 |
| Radius[m] | 0.60 | 0.90 | 0.84 | 0.71 | 0.71 |
| $n_b$ | 6 | 10 | 9 | 9 | 9 |
| Root foil | 1 | 6 | NACA 4415 | NACA 4412 | NACA 4412 |
| Tip foil | 1 | 6 | NACA 4412 | NACA 4412 | NACA 4412 |
| Foil change | 4 | 14 | 2 | n/a | n/a |
| $B_A$ | 92.0 | 115.0 | 107.6 | 96.3 | 96.3 |
| $B_B$ | -170.0 | -150.0 | -163,8 | -167.7 | -167.7 |
| $B_C$ | 69.0 | 84.0 | 69.0 | 83.6 | 83.6 |
| $\phi_A$ | -2.9 | -0.9 | -2.6 | -0.9 | -0.9 |
| $\phi_B$ | 2.0 | 9.0 | 4.6 | 2.0 | 2.0 |
| $c_A$ | -0.52 | -0.30 | -0.48 | -0.42 | -0.42 |
| $c_B$ | 0.18 | 0.33 | 0.33 | 0.29 | 0.29 |
| $c_C$ | 0.05 | 0.21 | 0.16 | 0.09 | 0.09 |

The database built contains only six airfoils [NACA 0012, NACA 4412, NACA 4415, NACA 0015, RAF 6, CLARK Y], that's the reason that the selection of airfoils varies from 1 to 6.

The criteria of evaluation were based on the sum of the thrust multiplied by the efficiency. The algorithm analyzed $5[m/s]$ above and below the cruise speed, considering the score in the cruise speed twice.

Figure 43: Thrust and torque of numerical BEMT results in ADE First Stage.

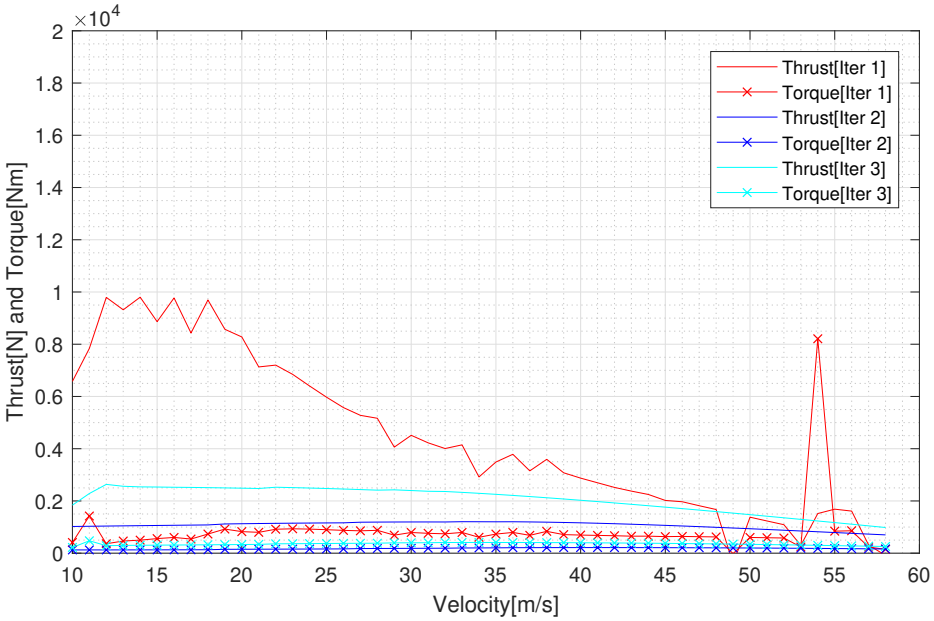


Source: Own authorship.

Figure 44: Propeller efficiency of numerical BEMT results in ADE First Stage.

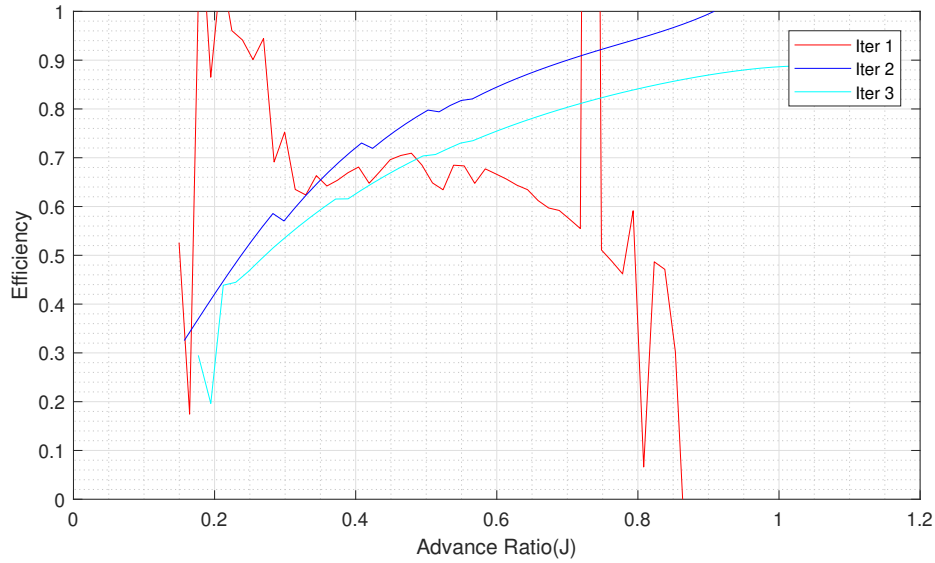


Source: Own authorship.

At first glance, it's possible to understand that this graphic doesn't represent the thrust and torque correctly, due to the abnormal results, Since efficiency is their reason is also plausible to conclude that it isn't reliable. So, based on the validation with experimental and analytical results in Chapter 6 it's normal to assume that this approach is reliable, however, the database built by the XFOIL is not for some airfoils. XFOIL in Mach next to 0.5, as mentioned earlier, has a limitation in these conditions.

### 7.1.2 Second Stage

Therefore, due to the understanding of the flaws in the database, the next step was optimizing the parameters of Xiang's propeller, since it operates at a lower Mach speed. So, the same process was made, setting the following parameters presented in Table 6 with the same limitations mentioned in the First Stage.

Table 6: Second Stage fixed parameters.

| Parameters | Value |
|---|---|
| $B$ | 2 |
| $n_b$ | 8 |
| Radius[m] | 0.80 |
| Foil change | 1 |
| $V$ | 37.6 |
| $\Omega$ | 1600 |

The criteria of evaluation were almost the same, the efficiency was not considered. The objective was to produce a higher thrust with a limited torque.

Table 7: Second stage ADE iteration results

| Parameters | Inferior limit | Superior limit | Iter 1 | Iter 2 | Iter 3 |
|---|---|---|---|---|---|
| Root foil | 1 | 6 | NACA 4415 | NACA 4412 | NACA 4412 |
| Tip foil | 1 | 6 | NACA 4415 | NACA 4412 | NACA 4412 |
| Foil change | 1 | 14 | n/a | n/a | n/a |
| $B_A$ | 95.0 | 115.0 | 104.90 | 101.94 | 101.94 |
| $B_B$ | -170.0 | -150.0 | -157.9 | -161.0 | -161.0 |
| $B_C$ | 69.0 | 84.0 | 75.07 | 76.80 | 76.80 |
| $\phi_A$ | -2.9 | -0.9 | -2.31 | -2.90 | -2.90 |
| $\phi_B$ | 2.0 | 9.0 | 5.53 | 8.13 | 8.13 |
| $c_A$ | -0.52 | -0.30 | -0.410 | -0.506 | -0.506 |
| $c_B$ | 0.18 | 0.33 | 0.219 | 0.314 | 0.314 |
| $c_C$ | 0.05 | 0.21 | 0.122 | 0.070 | 0.070 |

The results are shown in Figure 45 and 46. For this problem, the main idea is finding the best propeller in cruise velocity, the three show great efficiency in cruise speed. Iter 2 and 3 converged to the same propeller parameters but were not considered the best due to the difference in lower speed thrust, so Iter 1 was considered the best considering all the factors. Normally, Iter 2 and 3 presented the same results, and both can be considered an optimum airscrew.

Figure 45: Thrust and torque of numerical BEMT results in ADE Second Stage.

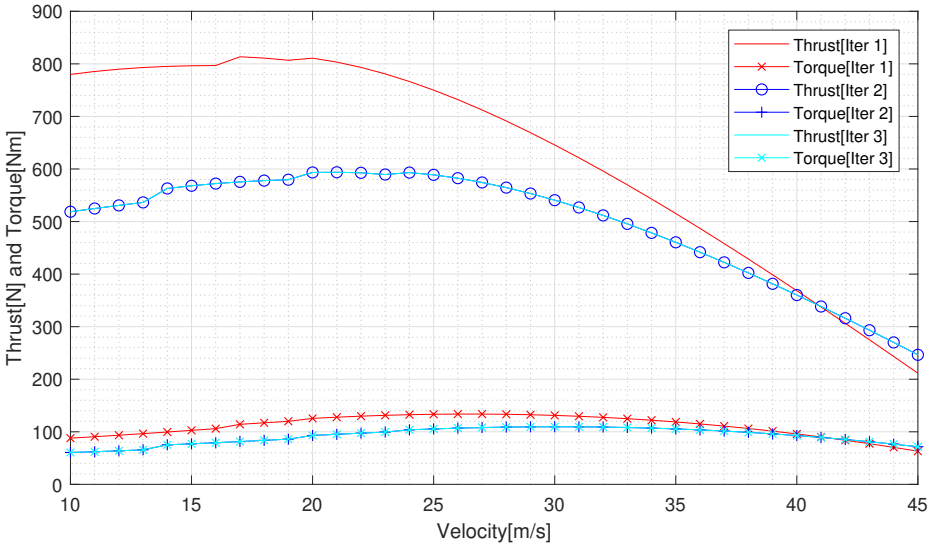


Source: Own authorship.

Figure 46: Propeller efficiency of numerical BEMT results in ADE Second Stage.

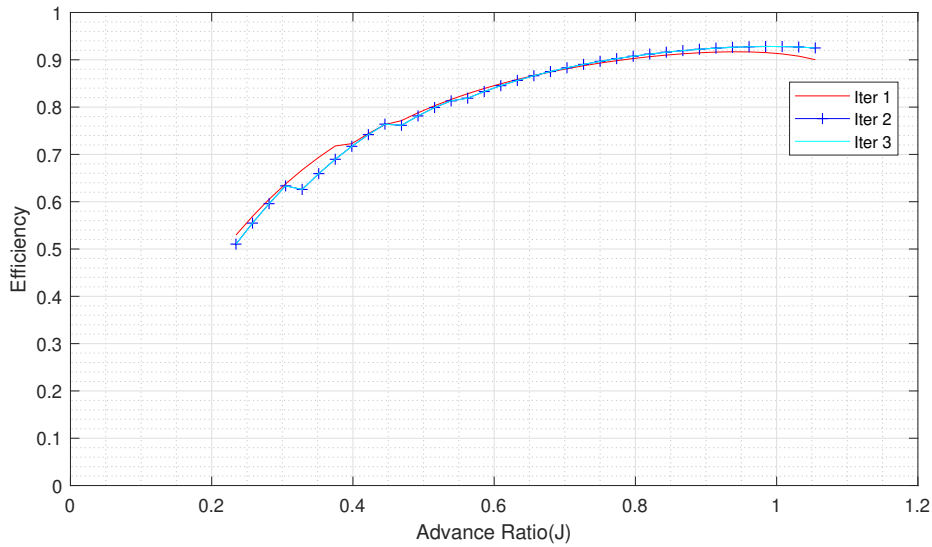


Source: Own authorship.

Finally, a comparison between the best propeller developed and the presented by Adkins is compared, to evaluate the improvement made by this approach, the results are presented below.

Figure 47: Thrust and torque comparison to Xiang's propeller.

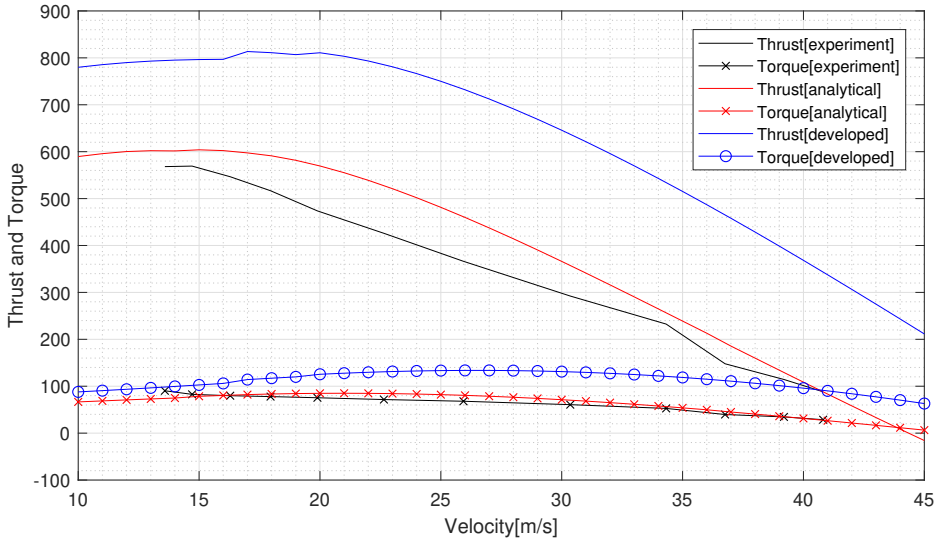


Source: Own authorship.

Figure 48: Propeller efficiency comparison to Xiang's propeller.

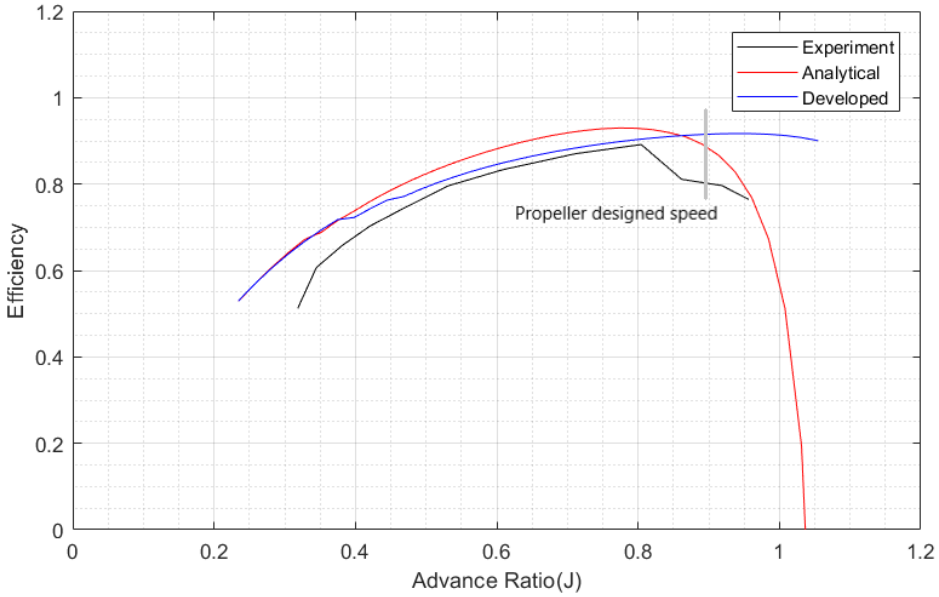


Source: Own authorship.

In conclusion, the propeller developed presented an efficiency 4% higher in comparison to the presented by Xiang[15], and even with the efficiency lower at low speeds, it was very close. Also, it's evident that the efficiency in higher speeds would be better and the thrust was higher, taking into consideration that the engine can support this torque.

# 8 Conclusion

The propeller analysis has been a success. In Chapter 6, the implementation of all equations presented brought a result undeniably good compared to the one presented by Adkins[2]. Since it was a validation of methodology, the next step was to compare the results with a real experiment, studied by Xiang[9], which also led to an algorithm result confirmation.

Once the model validated, it was proposed a methodology of an optimization algorithm Accelerated Differential Evolution in Chapter 5, which seemed to be promising for this analysis. Therefore, Chapter 7 shows the optimized propeller for all the cases, presented in Figures 48 and 47 that have higher thrust and 4% efficiency higher in the speed stipulated. Finally, considering all the statements realized, it's possible to claim that it's a great approach to optimize the propeller in the first stages of development.

Even though the modeling of propeller performance calculations showed an excellent result, to further enhance the propeller studies some implementations can be made:

- Implement a constant speed propeller configuration.
- A hub analysis can approach the analytical result to experiments.
- Another method to acquire data seems more reliable to Mach higher than 0.4 because even with reliable XFOIL data, the results showed a controversial statement, especially because compressibility effects become more significant after this value.
- At low advance ratio values, thrust, and torque curves exhibit oscillations. These oscillations are attributed to significant blade stall conditions, prompting the use of the Viterna method to approximate the aerodynamic coefficients. The potential for improving this approximation by exploring alternative methods is worth consideration.
- A model of noise and vibrations could be also introduced to study these parameters that are important to qualification in norms.
- Previous structural limits studies of propeller resistance can improve the reliability of constructing it.
- CFD models can analyze propellers with higher accuracy.
- Acquisition of more airfoils to build the database can be considered.

# References

[1] Anacpedia. Available on: https://medium.com/how-to-aviation/understanding-parasite-and-induced-drag-e629dd97997e. Accessed on may 2023.

[2] Adkins, C. N., and Liebeck, R. H. Design of optimum propellers. *Journal of Propulsion and Power 10* (1994), 676–682.

[3] Anderson, J. D. *Fundamentals of Aerodynamics*. McGraw-Hill, 2011.

[4] Drela, M. *XFOIL - An analysis and design system for low Reynolds number airfoils*. Mueller T.J. (eds) Low Reynolds Number Aerodynamics. Lecture Notes in Engineering, Vol. 54, 1989.

[5] Glauert, H. *Airplane propellers*. W.F.Durand, 1935.

[6] Harris, C. D. *Two dimensional characteristics of the NACA 0012 airfoil in the Langley 8-foot transonic pressure tunnel*. NASA TM-81927, 1981.

[7] Hitchens, F. E. *Propeller Aerodynamics: The history, aerodynamics Operation of Aircraft Propellers*. Andrews UK Limited, 2015.

[8] Mahmuddina, F. Airfoil lift and drag extrapolation with viterna and montgomerie methods. Available on: https://doi.org/10.1016/j.egypro.2017.03.394, 2017.

[9] Martins, J. R. R. A., and Ning, A. *Engineering Design Optimization*. Cambridge University Press, 2020.

[10] Martín, J. d. Z. Optimal design methods with choice of aerodynamic profiles for aircraft propellers. Master's thesis, Politecnico di Milano, 2020.

[11] Ning, S. A. A simple solution method for the blade element momentum equations with guaranteed convergence. Available on: https://doi.org/10.1002/we.1636, Sep. 2014.

[12] Sadraey, M. H. *Aircraft Performance: An Engineering Approach*. CRC Press, 2017.

[13] Tarraran, N. Optimal approach to propeller design. Available on: https://hdl.handle.net/10589/138698, 2018.

[14] Viterna, L. *Fixed pitch rotor performance of large horizontal axis wind turbines*. NASA TR-19830010962, 1982.

[15] Xiang, S., Liu, Y.-q., Tong, G., Zhao, W.-p., Tong, S.-x., and Li, Y.-d. An improved propeller design method for the electric aircraft. *Aerospace Science and Technology 78* (2018), 488–493.

[16] Çengel, Y. A., and Cimbala, J. M. *Fluid Mechanics: Fundamentals and Application*, 3 ed. McGraw-Hill, 2014.